Mechanical Design of Flow Batteries

by

Brandon J. Hopkins

B. A. Mechanical Engineering
Harvard University, 2011

SUBMITTED TO THE DEPARTMENT OF MECHANICAL ENGINEERING IN PARTIAL FULFILLMENT OF THE REQUIREMENTS OF THE DEGREE OF

MASTER OF SCIENCE IN MECHANICAL ENGINEERING AT
MASSACHUSETTS INSTITUTE OF TECHNOLOGY
MAY 2013
[JUNE 2013]

Signature of Author _____

Brandon J Hopkins
Department of Mechanical Engineering
May 16, 2013

Certified by _____

Alexander H. Slocum
Pappalardo Professor of Mechanical Engineering
Thesis Supervisor

Accepted by _____

David E. Hardt
Ralph E. and Eloise F. Cross Professor of Mechanical Engineering
Chairman, Committee for Graduate Students

Mechanical Design of Flow Batteries

by

Brandon J. Hopkins

Submitted to the Department of Mechanical Engineering
on May 16, 2013 in partial fulfillment of the requirements for the degree of
Master of Science in Mechanical Engineering

ABSTRACT

The purpose of this research is to investigate the design of low-cost, high-efficiency flow batteries. Researchers are searching for next-generation battery materials, and this thesis presents a systems analysis encompassing static and moving electrode architectures that identifies which architecture is most appropriate for which materials and how to modify those materials to decrease cost and increase efficiency. The cost model and mechanical designs presented will help researchers (*i*) identify how to modify existing materials, (*ii*) find new desirable materials, and (*iii*) use those materials in novel flow battery structures to create next-generation batteries.

Thesis Supervisor: Alexander H. Slocum
Title: Pappalardo Professor of Mechanical Engineering

Acknowledgments

I thank and acknowledge God as the source of all things that are good and true. I am grateful to my parents, Barbara and James Hopkins, who have given their all to me. I thank my professor, Alexander H. Slocum whose academic teaching and personal example have had a profound impact on me. I appreciate professors Yet-Ming Chiang and Craig Carter for their guidance on the electrochemical aspects of this research. I give a special thanks to Christian Höcker, Victor Brunini, Yajie Dong, Kyle Smith, Zheng Li, and Nir Baram for being wonderful teammates. Thank you all very much.

Table of Contents

List of Figures

List of Tables

Chapter 1

Introduction

1.1 Research Objectives

The purpose of this research is to investigate the design of flow batteries and attempt to create a design that costs less than $100/kWh and has an energetic efficiency greater than 95%. Researchers are searching for next-generation battery materials, but no systems analysis encompassing static and moving electrode architectures has been performed that identifies which architecture is most appropriate for which materials and how to modify those materials to decrease cost and increase efficiency. The cost model and mechanical designs presented herein will thus help researchers (*i*) identify how to modify existing materials, (*ii*) find new desirable materials, and (*iii*) use those materials in novel flow battery structures to create next-generation batteries.

1.2 Need for Low-Cost, High-Efficiency Energy Storage

Low-cost, high-efficiency energy-storing systems are critical to expanding the integration of renewable energy sources into the US power grid. Currently the grid is unable to store significant excess energy, meaning that electrical energy must be constantly generated to meet immediate demand. Unlike coal and natural gas that can be used to generate electrical energy on demand, renewable energy sources generate unpredictable and intermittent power. The lack of

energy storage in the grid decreases the amount of energy that can be used from the intermittent renewable energy sources, which is why over 70% of US electricity generation comes from coal and natural gas [1] [2]. The few energy storage facilities available in the US use pumped hydropower, which is, however, only available in several locations. The current cost goal of such energy storage systems is $100/kWh, or one fourth the cost of standard lithium-ion batteries [3]. Expanding the integration of renewable energy sources into the US grid would (*i*) make the US a more independent global energy leader, (*ii*) decrease carbon dioxide emissions, (*iii*) decrease the demand and consequently the price of fossil fuels, and (*iv*) generate high-paying jobs in the US energy sector.

1.3 Flow Batteries

Flow batteries have the potential to become a low-cost, high-efficiency energy-storing system. The economic benefits of flow batteries can be explained by analogy. Imagine that a group of people must travel a long distance. One option for transporting the people is to purchase a motorcycle for every individual in the group. Another option is to purchase one large bus big enough for everyone in the group. Assume that in order to distribute the economic burden fairly, every individual contributes an equal amount of money to transportation. The sum of everyone's contribution is equal to the total cost of transportation. The cost of transport per individual for the motorcycle option stays constant as more individuals join the group. The more people that join the group, the more motorcycles are required. For the bus option, however, the more people that join the group, the lower the cost per individual because only one bus must be purchased to allow the whole group to travel. If the group is small, the motorcycle option would be lower cost. If the group is large, the bus option would be lower cost. In this analogy, the motorcycle option is storing energy using conventional batteries, and the bus option is storing energy using a flow battery.

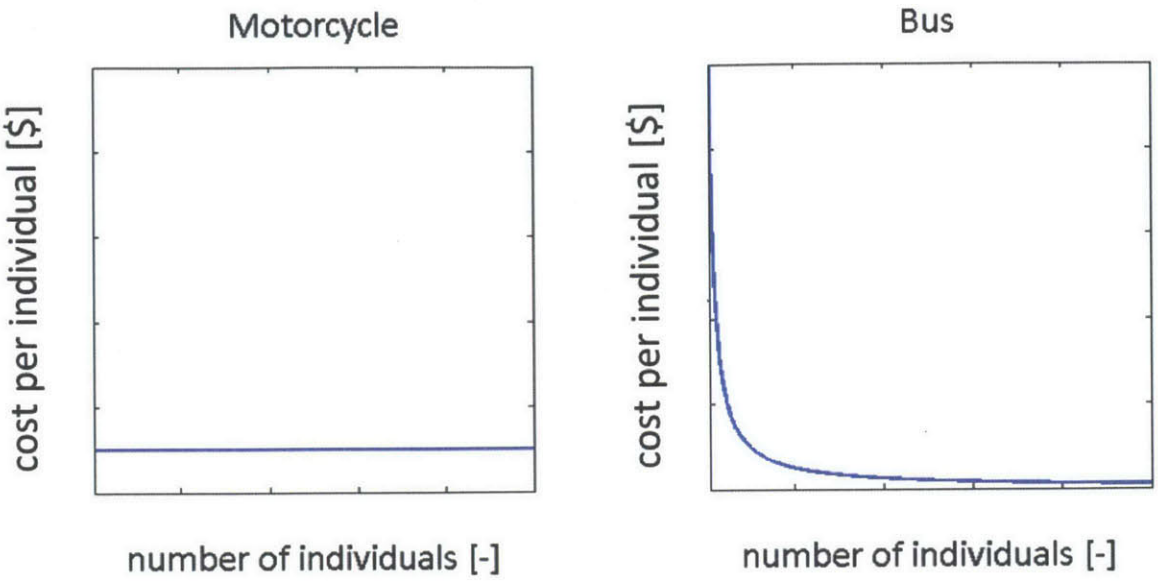

Figure 1.1: Graphical Interpretation of Analogy

The passengers are the chemically active anode and cathode material that store energy. The membrane and current collector in the battery is the motorcycle or bus. Flow batteries have the potential to be lower cost than conventional batteries if the membrane and current collector required for anode and cathode material are relatively costly. The flow battery architecture decreases the amount of membrane and current collector used in the battery by having the anode and cathode material move past the membrane and current collector, or vice versa. The anode and cathode material in conventional batteries, however, does not move, and so for the anode and cathode material to be useful, it must always be surrounded by membrane and current collector material, which in turn requires more membrane and current collector material. Flow batteries, however, require mechanisms to move the anode and cathode material relative to the membrane and current collector region, which in itself requires energy to operate and adds mechanical complexity to the system.

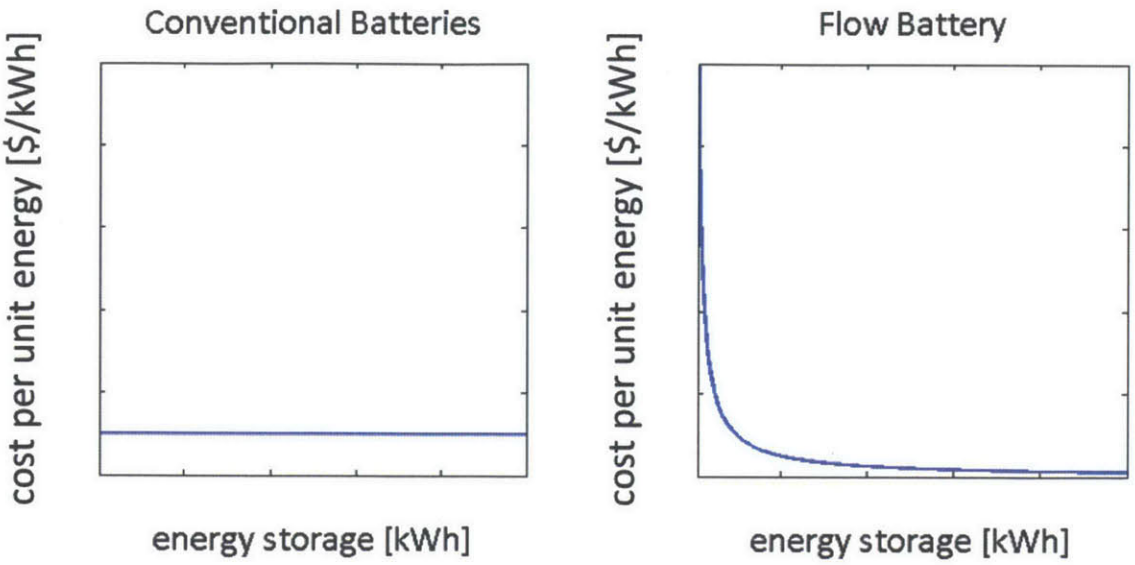

Figure 1.2: Graphical Comparison of a System of Conventional Batteries vs. a Flow Battery

Figure 1.3, shows a diagram of a flow battery. A conventional battery is essentially a flow battery without the pumps or storage tanks. In a conventional battery, all anode and cathode material is stored between the separator membrane and current collectors.

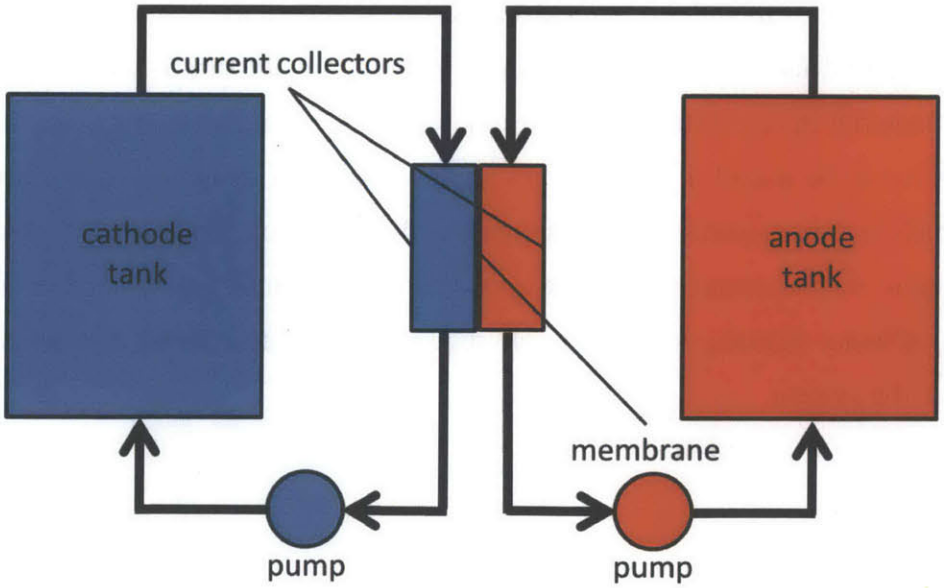

Figure 1.3: Flow Battery Architecture

Flow batteries also have the potential to be more energy dense than conventional batteries. The cost of the infrastructure of conventional batteries scales linearly with the amount of energy stored in the battery and can decrease the amount of energy stored per mass by one-half. For example, lithium-ion batteries use active materials that have high energy densities, approximately 400 Wh/kg. Once the supporting inactive materials are taken into account, however, the energy density on a system level is 120-200 Wh/kg [4]. The cost of the infrastructure of flow batteries, however, does not scale as steeply with increased stored energy as conventional batteries, and so they have the potential to be more energy dense than conventional batteries, if the desired energy storage is sufficiently large.

1.4 Suspension-Based Flow Batteries

Suspension-based flow batteries were created by Chiang in 2010 [5] [6] and are one of many types of flow batteries that are being researched [7]. The key feature that distinguished suspension-based flow batteries from other flow batteries is that carbon black is suspended in the anode and cathode material making the material electrically conductive. The anode and cathode materials of many other flow batteries are only ionically conductive. For other flow batteries, an electrically conductive carbon felt can be placed between the membrane and current collector, and the anode and cathode material can be pumped through the carbon felt. In suspension-based flow batteries, no carbon felt is needed because the carbon black in effect acts as a carbon felt that is evenly distributed throughout the anode and cathode material allowing electrochemical reactions to occur throughout the materials. The unique mechanical consequences of the ionic conductivity of the suspension-based flow batteries will be explored in Chapter 3. Chapter 2 explains how to determine when it is economically appropriate to use a flow battery architecture for a given set of materials.

Chapter 2

Static vs. Moving Electrode Architecture Cost Model

2.1 Chapter Overview

This section presents a cost model that identifies what chemistries could be economically used in flow-battery architectures. The cost analysis demonstrates that flow, or moving electrode, battery architectures are only desirable if the cost of the membrane and current collector are high relative to the cost of the anode and cathode material in conventional, static electrode, architectures. Decreasing membrane and current collector cost and increasing anode and cathode conductivity diminish the advantages of the flow battery architecture. This analysis guides electrochemists to properly modify existing battery materials and to identify new, desirable materials to study that could be economically desirable to use in moving electrode architectures. Cost-analyses of suspension-based (*i*) aqueous lithium iron phosphate (LFP)/ lithium titanium phosphate (LTP), (*ii*) non-aqueous lithium iron phosphate (LFP)/ graphite, and (*iii*) all-vanadium chemistries are presented. All-vanadium suspension-based chemistries are identified as having the most economic potential in moving electrode architectures of the three anode and cathode materials studied.

2.2 Independent Variables

A goal of this research is to create a moving electrode battery with a cost per unit energy less than $100/kWh that has an energetic efficiency greater than 95%. Multiple independent variables affect the cost per unit energy and the energetic efficiency of a flow battery. The following outline summarizes some key independent variables and how these variables are dealt with in the cost analysis.

Independent Variables Taken into Account by Model

A. Anode & Cathode Material
   - Density of anode and cathode material [kg/m^3]
   - Cost of anode and cathode [$]
   - Combined gravimetric energy density of anode and cathode material [kWh/kg]
   - Conductivity of carbon black chemistries [S/m]

B. Membrane & Current Collector
   - Cost of membrane and current collector [$]

C. Battery Specifications
   - C-rate, reciprocal of the time used to discharge a battery [h^{-1}], assumed to be 1/12
   - Electrode thickness, distance from membrane to current collector [m]

D. Battery Operation
   - Temperature of operation, assumed to be constant at 293 K

Independent Variables Not Taken into Account by Model

A. Battery Structure
   - Cost of materials excluding anode and cathode material, membrane, and current collector

B. Battery Operation
   - Cost to move anode and cathode material relative to membrane and current collector

2.3 Static vs. Moving Electrode Architecture Cost Model

The term "static electrode architecture" refers to the architecture of conventional batteries whose anode and cathode material do not move relative to the membrane and current collector. The term "moving electrode architecture" is used to refer to the flow battery architecture in which the anode and cathode material move relative to the membrane and current collector. The term "moving" is used instead of "flow" to highlight the fact that the anode and cathode material need not flow to be in moving electrode architectures. The moving electrode architecture and benefits can be thought of as is independent of the anode and cathode's thermodynamic phase or viscoelastic properties. Also the anode and cathode need not move in the reference frame of an observer. The membrane and current collector can move instead.

While the moving electrode architecture used in flow batteries has potential to yield low-cost batteries by decreasing the amount of required membrane and current collector, conventional batteries use a static electrode architecture that requires no moving parts or operating costs. The designer therefore must determine if the moving electrode architecture, which requires a more complicated infrastructure, is merited. This section outlines the derivation of an analytical equation that captures the theoretical maximum possible difference in cost per unit energy between a battery using a static electrode architecture and a battery using a moving electrode architecture assuming that both batteries (*i*) use the same anode and cathode material, current collector, and separator membrane, (*ii*) have the same energetic efficiency and charging and discharging C-rate, and (*iii*) have a negligible casing, operations, and maintenance cost. Rheology of the anode and cathode material is not taken into account in this analysis because the anode and cathode materials need not flow or be a fluid to be used in moving electrode architecture. It will therefore also be assumed that (*iv*) moving the anode and cathode material requires no energy and causes no release of energy or loss in efficiency.

By assuming (*i*) through (*iv*), one insures that the derived difference in cost per unit energy between the static and moving electrode batteries is as large as possible. Determining the maximum possible difference in cost between a static and a moving electrode architecture allows one to identify the maximum possible gain achievable by switching from a static to a moving

electrode design. If the theoretical maximum price difference is small, a moving electrode architecture is not merited.

$$C_{E,p} = \frac{(C_{AC} + C_M + C_C + C_S + C_O)}{E} \tag{2.1}$$

$C_{E,p}$ = [$/kWh] cost per unit energy of static or moving electrode battery

C_{AC} = [$] total cost of anode and cathode material

C_M = [$] total cost of membrane

C_C = [$] total cost of current collector

C_S = [$] total cost of structure defined as all other materials associated with the battery excluding the anode and cathode material, membrane, and current collectors

C_O = [$] total cost of operation and maintenance

E = [kWh] total usable energy output

For the purposes of this analysis, assume that C_S, and C_O are negligibly small in comparison to the cost of the other components of the battery. Define the following variables.

$$C_{AC} = \frac{P * c_{AC}}{C * \rho_{E,O} * \alpha_C} \tag{2.2}$$

P = [kW] average charging power

c_{AC} = [$/kg] cost average of anode and cathode per unit mass

C = [1/h] C-rate at which battery charges and discharges

$\rho_{E,O}$ = [kWh/kg] theoretical gravimetric energy density

α_C = normalized charging gravimetric energy density

eff = [-] energetic efficiency = $\frac{useable\ energy\ output}{total\ energy\ input}$

$$C_M = A_M * c_M \tag{2.3}$$

A_M = [m^2] total area of membrane

c_M = [\$/m^2] membrane cost per unit area

$$C_C = A_C * c_C \tag{2.4}$$

A_C = [m^2] total area of current collector

c_C = [\$/m^2] current collector cost per unit area

$$E = \frac{P * eff}{C} \tag{2.5}$$

Equation 2.6 through 2.10 show the derivation of the amount of membrane and current collector required to achieve a specified average power and energy storage.

$$A_C = A_M * \left(1 + \frac{1}{n}\right) \tag{2.6}$$

n = [-] number of cells in the battery assuming cells are stacked side by side and share current collectors

Moving electrode batteries differ from static electrode batteries in that they require less membrane and current collector area to achieve the same power and energy. The trade-off, however, is that the C-rate of the plugs of material that move relative to the membrane and current collector must be charged and discharged at higher C-rates in order to achieve a net C-rate equal to that of a static electrode battery. The C-rate of an individual plug is defined in Equation 2.7.

$$C_p = C * p \tag{2.7}$$

C_p = [1/h] C-rate at which one plug in a moving electrode battery charges and discharges

p = [-] plug count

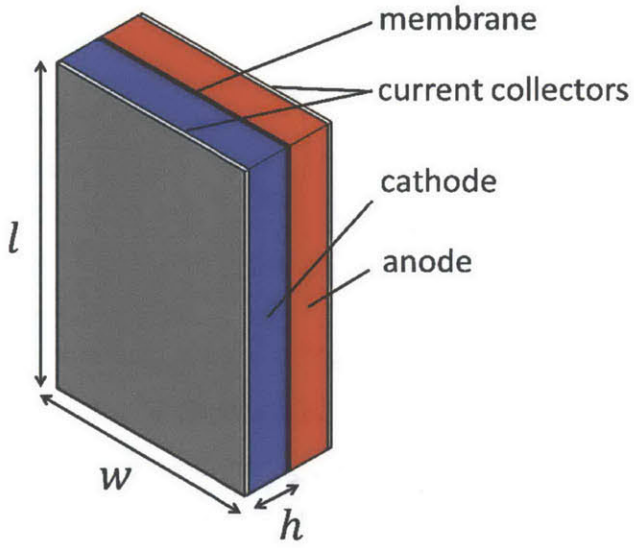

Figure 2.1: Single Cell Diagram

$$P = (2 * h * l * w) * \rho * \rho_{E,O} * \alpha_C * C_p * n \tag{2.8}$$

h = [m] electrode thickness or distance from membrane to current collector as shown in Figure 2.1, a function of eff and C

l = [m] length of current collector as shown in Figure 2.1

w = [m] width of current collector as shown in Figure 2.1

ρ = [kg/m^3] average density of anode and cathode material

Divide both sides of Equation 2.7 by A_M, the total area of required membrane, which is equal to $l * w * n$, and solve for A_M.

$$A_M = \frac{P}{2 * h * \rho * \rho_{E,O} * \alpha_C * C_p} \tag{2.9}$$

Substitute Equations 2.2 through 2.7 and Equation 2.9 into Equation 2.1.

$$C_{E,p} = \left(\frac{1}{eff * \rho_{E,O} * \alpha_C}\right) * \left(c_{AC} + \frac{c_M + c_C * \left(1 + \frac{1}{n}\right)}{2 * h * \rho * p}\right) \tag{2.10}$$

Equation 2.10 expresses the cost per unit energy of a static electrode design when $p = 1$ and the cost per unit energy of a moving electrode design when $p > 1$, meaning a moving electrode battery is identical to a static electrode battery, given the previously stated assumptions, when only one plug of anode and cathode material is present. The maximum achievable cost difference between a static and moving electrode battery is calculated by subtracting the cost per unit energy when $p = 1$ and the cost per energy when $p = \infty$ using Equation 2.10. Three main conclusions can be made by understanding Equation 2.10.

Conclusion 1

Moving electrode architectures are only justified when the relative cost of membrane and current collector are high in the static electrode architecture design. As the variable p, the plug count, goes to infinity, the amount of membrane and current collector needed goes to zero as can be seen in Equation 2.9. If the cost of the membrane and current collector in the static architecture design, i.e. when $p = 1$, is small, little cost reduction is achieved by decreasing the amount of membrane and current collector required by switching to a moving electrode architecture, i.e. when $p > 1$. Therefore, battery materials are economical to use in a moving electrode design only if the relative cost of the membrane and current collector are high in the static electrode design assuming the same materials are used in both architectures.

Conclusion 2

Moving electrode architectures can be avoided by (*i*) decreasing membrane and current collector cost and /or (*ii*) increasing anode and cathode conductivity. The first option (*i*) follows from the logic presented in first conclusion. The second option (*ii*) decreases the amount of membrane and current collector needed to achieve the same cost per unit energy. As the conductivity of anode and cathode material increases, the allowable electrode thickness, h, increases while maintaining the same energetic efficiency. As the allowable electrode thickness increases, the amount of current collector and membrane required decreases as can be seen in Equation 2.9. Increasing the electrical conductivity of the anode and cathode effectively decreases the relative cost of the membrane and current collector in both moving and static electrode designs.

Conclusion 3

The difference in cost between a static and moving electrode battery that use the same amount of anode and cathode material is independent of the cost of anode and cathode material. If it is assumed that there are no inefficiencies associated with the moving electrode architecture that are not found in the static architecture, the amount of anode and cathode used in a static and moving electrode architecture will be identical and the difference in cost between them will therefore be dictated by the cost of the membrane and current collector. Granted, as the cost of the anode and cathode material decreases, (*i*) the total cost of the battery decreases and (*ii*) the percentage decrease in price achieved by switching from static to moving architectures will increase.

If the cost of membrane and current collectors significantly decreases in comparison to the cost of anode and cathode materials, the benefits of the flow battery architecture could become obsolete because the incremental theoretical possible price drop allowed for by the flow battery architecture could be outweighed by the practical benefits of a static battery architecture that requires no moving parts. It should also be stressed that there are a variety of reasons why a moving electrode battery could not feasibly be designed with a high p value. The main purpose of this cost model is to quantitatively bound the maximum possible gains achieved by switching from a static to a moving electrode architecture.

2.4 Sensitivity Analysis Results

The following cost-analysis examples will be discussed using suspension-based (*i*) aqueous lithium iron phosphate (LFP)/ lithium titanium phosphate (LTP), (*ii*) non-aqueous lithium iron phosphate (LFP)/ graphite, and (*iii*) all-vanadium chemistries. All-vanadium suspension-based chemistries were identified as having the greatest economic potential of those studied in moving electrode architectures.

Tables 2.1 and 2.2 outline the values used in the cost analysis. Figures 2.2 through 2.4 show sensitivity curves generated by a simulated model of battery electrochemistry. The in-house simulation model was created by Kyle C. Smith. Table 2.3 combines the data found in Tables 2.1 and 2.2 and from Figures 2.3 through 2.4 to calculate the cost per unit energy of each battery and the percentage cost contribution of anode and cathode material and associated membrane and current collector cost. Table 2.4 shows the cost of static electrode batteries and the lowest possible cost of a moving electrode battery using the same materials in both architectures.

Battery Materials	kg/m^3	$/kg	Ah/kg
Carbon Black	2267	~ 0	N/A
H_2O	1000	~ 0	N/A
H_2SO_4	1840	~ 0	N/A
SSDE	1310	60	N/A
Vanadium	6000	21	33
LFP	3570	15	150
LTP	2950	15	120
Graphite	2230	10	280

Table 2.1: Battery Material Properties [8]

Cathode/Anode	Voltage [V]	Current Collector [$/m^2]	Membrane [$/m^2]
Aqueous LFP/LTP	1	0.5	2
Non-aqueous LFP/Graphite	3.3	0.5	2
All-Vanadium Suspension Based	1.3	51	500

Table 2.2: Anode and Cathode Properties and Membrane and Current Collector Costs [9]

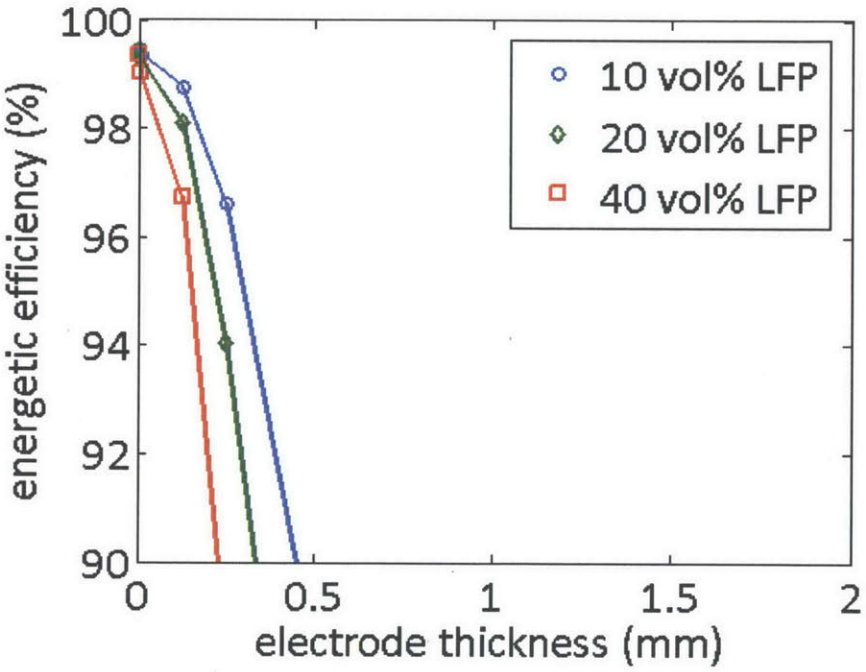

Figure 2.2: Aqueous 10 vol% LFP/15 vol% LTP, Aqueous 20 vol% LFP/30 vol% LTP, Aqueous 40 vol% LFP/60 vol% LTP, C-rate 1/12 h^{-1}, conductivity 0.01 S/m

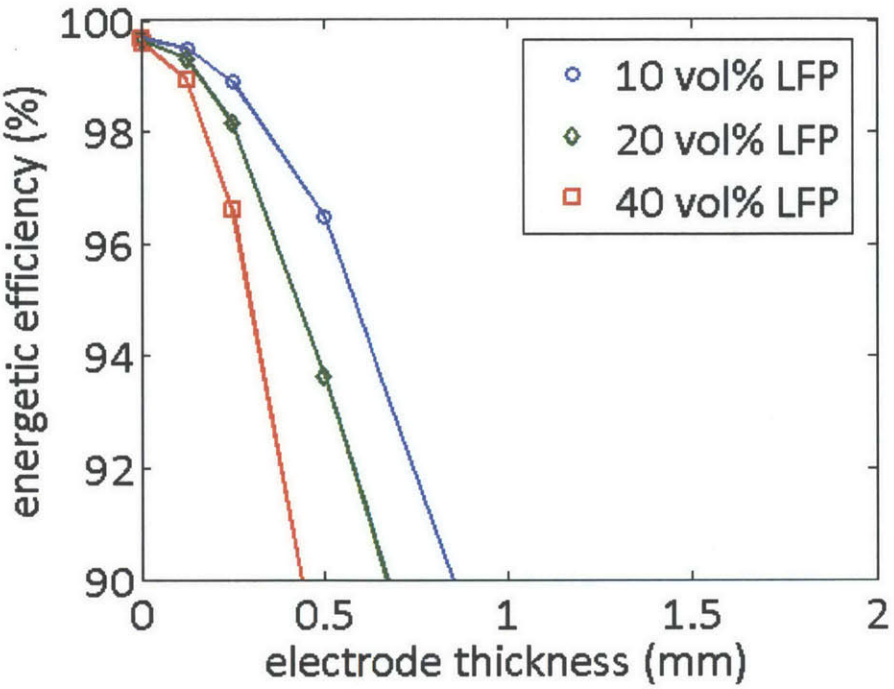

Figure 2.3: Non-aqueous 10 vol% LFP/8 vol% Graphite, Non-aqueous 20 vol% LFP/17 vol% Graphite, Non-aqueous 40 vol% LFP/34 vol% Graphite, C-rate 1/12 h^{-1}, conductivity 0.01 S/m

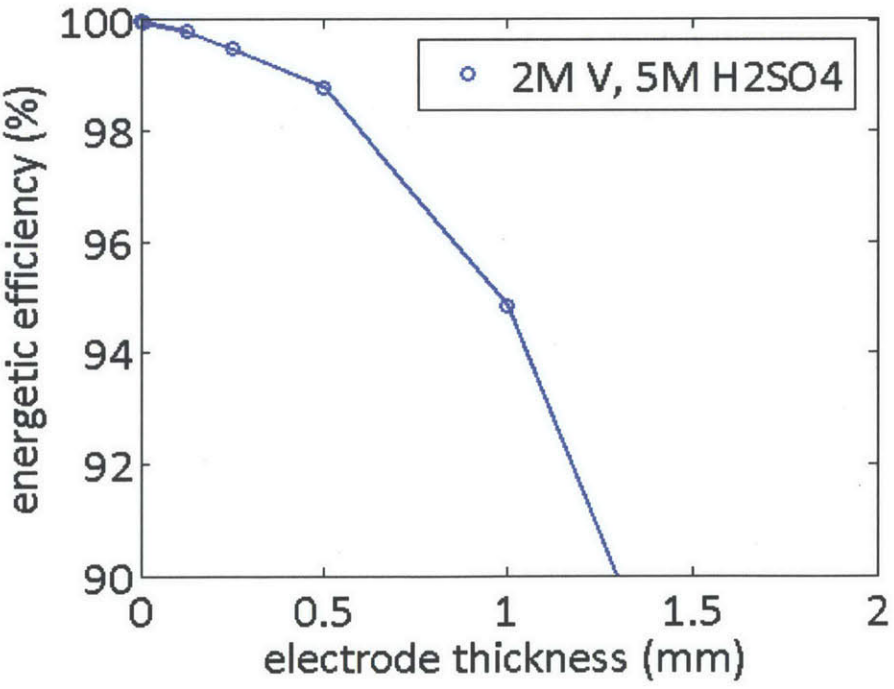

Figure 2.4: 2M Vanadium, 5M Sulfuric Acid, C-rate 1/12 h^{-1}, conductivity 0.01 S/m

Cathode/Anode	$/kg	Wh/kg	Wh/L	h [μm]	$/kWh	% cost membrane and current collector
Aq. 10 vol% LFP/15 vol% LTP	5	21	16	350	377	38
Aq. 20 vol% LFP/30 vol% LTP	8	34	22	300	318	26
Aq. 40 vol% LFP/60 vol% LTP	11	50	24	250	285	17
Non-aq. 10 vol% LFP/ 8 vol% Graphite	50	58	39	600	933	3
Non-aq. 20 vol% LFP/ 17 vol% Graphite	43	108	66	500	434	4
Non-aq. 40 vol% LFP/ 34 vol% Graphite	33	182	94	400	198	5
2M Vanadium, 5M H_2SO_4	1	42	27	1000	4347	99

Table 2.3: Summary of Calculated Battery Specifications, $/kWh for Static Electrode Architecture, 2 vol% Carbon Black Assumed in All Cathode/Anode Pairs

The values in the "% cost membrane and current collector" column of Table 2.3 quantify the potential for using material in moving electrode architectures. The greater the percentage cost of the membrane and current collector, the greater the economic potential will be of using a particular anode and cathode material in a moving electrode architecture.

Cathode/Anode	$/kWh Static ($p = 1$)	$/kWh Moving ($p = \infty$)
Aq. 10 vol% LFP/15 vol% LTP	377	236
Aq. 20 vol% LFP/30 vol% LTP	318	236
Aq. 40 vol% LFP/60 vol% LTP	285	236
Non-aq. 10 vol% LFP/8 vol% Graphite	933	907
Non-aq. 20 vol% LFP/17 vol% Graphite	434	419
Non-aq. 40 vol% LFP/34 vol% Graphite	198	189
2M Vanadium, 5M H_2SO_4	4347	33

Table 2.4: Best Case Scenario of Cost per Unit Energy of Static and Moving Electrode

Table 2.4 shows that the all-vanadium suspension-based material has the greatest economic potential in the flow battery architecture. The non-aqueous LFP/Graphite material has the lowest potential, and the aqueous LFP/LTP material has a moderate economic potential. The simulation data also shows that as the conductivity of the anode and cathode material increases, the amount of necessary membrane and current collector material decreases as shown by Equation 2.9. Therefore, if the conductivity of the anode and cathode material can be significantly increased, the moving electrode architecture can be avoided. Figure 2.5 shows the effect of increasing conductivity on allowable electrode thickness in the case of aqueous LFP/LTP. Non-aqueous LFP/Graphite and all-vanadium materials follow similar trends. The simulations show theoretical results for specified conductivities. More experimentation would have to be performed to determine if these conductivities could actually be achieved by suspending more carbon black in the anode and cathode materials.

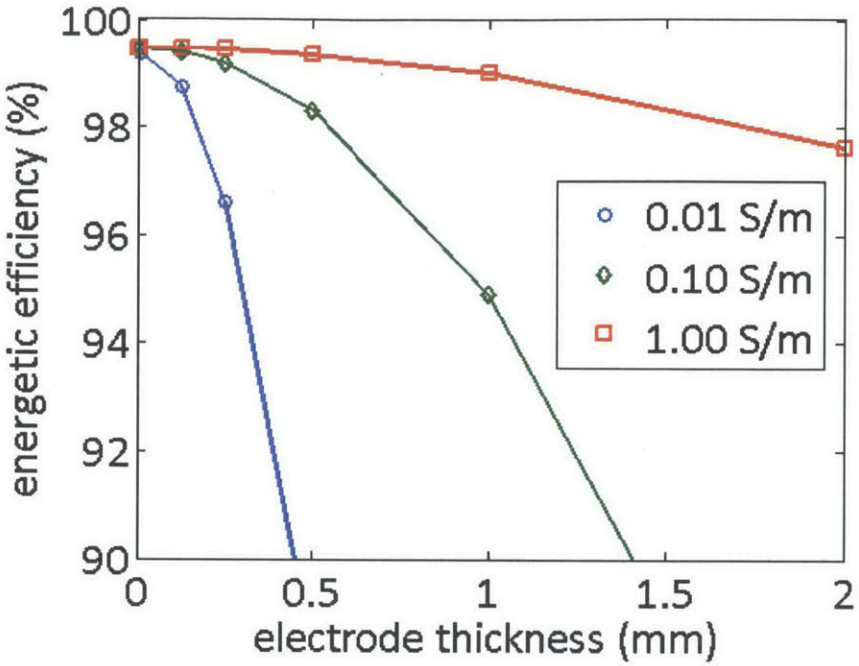

Figure 2.5: Aqueous 10 vol% LFP/15 vol% LTP, C-rate 1/12 h^{-1}

2.5 Chapter Summary

This section presents a cost model that identifies which chemistries have the greatest economic potential in conventional or flow battery architectures. The cost analysis demonstrates that moving electrode architectures are desirable only if the cost of the membrane and current collector is high relative to the cost of the anode and cathode material in static electrode architectures. The complexity of moving electrode architectures can be avoided by decreasing membrane and current collector cost and increasing anode and cathode conductivity. This analysis can guide electrochemists to properly modify existing battery materials and to identify new desirable materials to study that could have great economical potential in moving electrode architectures. Cost-analysis using suspension-based (*i*) aqueous lithium iron phosphate (LFP)/ lithium titanium phosphate (LTP), (*ii*) non-aqueous lithium iron phosphate (LFP)/ graphite, and (*iii*) all-vanadium chemistries are presented. All-vanadium suspension-based chemistries are identified as having economic potential in moving electrode architectures.

Chapter 3

Mechanical Design of Suspension-Based Flow Batteries

3.1 Chapter Overview

This section investigates the mechanical design of suspension-based flow batteries. The mechanical design of conventional flow batteries is presented for comparison. New concepts for conventional flow battery architectures are outlined. Prior art and design requirements for suspension-based flow batteries are specified.

3.2 Mechanical Design of Conventional Flow Batteries

Figure 3.1 shows the Skyllas-Kazacos et al. 1988 patent drawing of the vanadium redox flow battery [10] that has become the only commercially produced redox flow battery since initial research started in the 1970s [11].

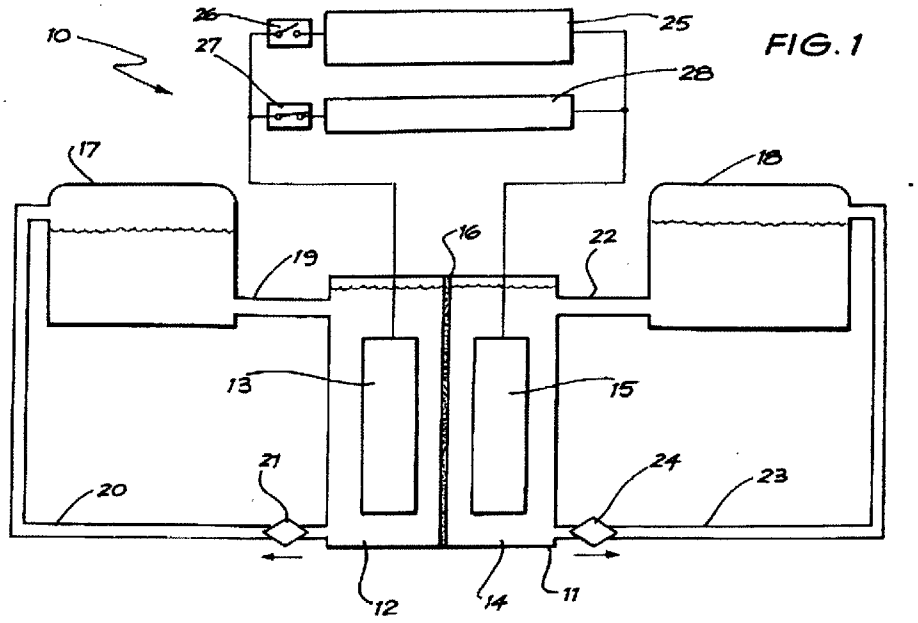

Figure 3.1: Vanadium Redox Flow Battery Mechanical Design [10]

Items 21 and 24 are pumps, and 17 and 18 are storage tanks. In the cell stack there is a separator membrane, 16, and electrodes, 13 and 15. Significant research since 1988 has yielded little change in the overall mechanical design. Current researchers have focused on creating control systems that ideally operate the battery by actively controlling the anode and cathode pumping speeds and temperature, which can improve the energetic efficiency of the battery by as much as 8% [12] [11] [13]. The pumps and heat exchanger used in the optimization of the battery make up 3% of the capital cost of the battery [9], and the pumping inefficiency and shunt current account for approximately 2-3% of the overall energetic efficiency [14]. The EnerVault Corporation mentioned a concept for a mechanical design in which flow is induced by gravity in a 2010 US patent [15]. A gravity induced flow battery is considered in this research and can be seen in Figure 3.2 through 3.5.

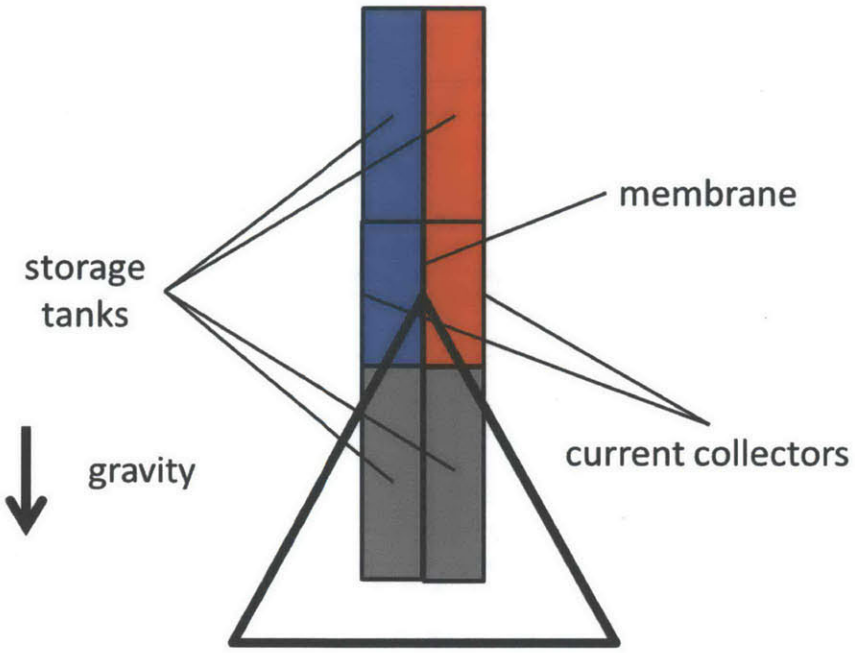

Figure 3.2: Gravity Induced Flow Battery

The fluid flows by gravity. The speed of the flow is controlled by the angle at which the battery is tilted with respect to the triangular stand. The grey storage tanks have no anode and cathode material in them and are the location where the anode and cathode material go as the battery is charged or discharged. Multiple geometries for this concept are possible.

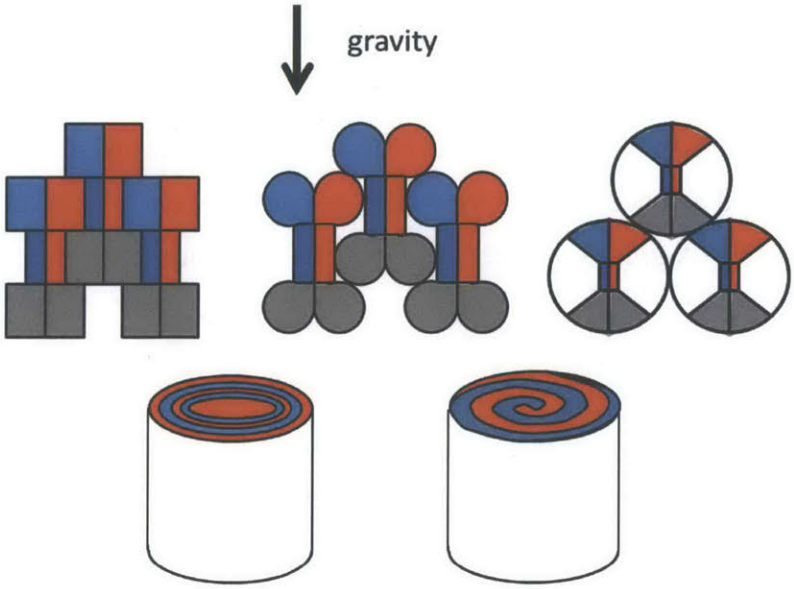

Figure 3.3: Gravity Induced Flow Battery Geometry Variations

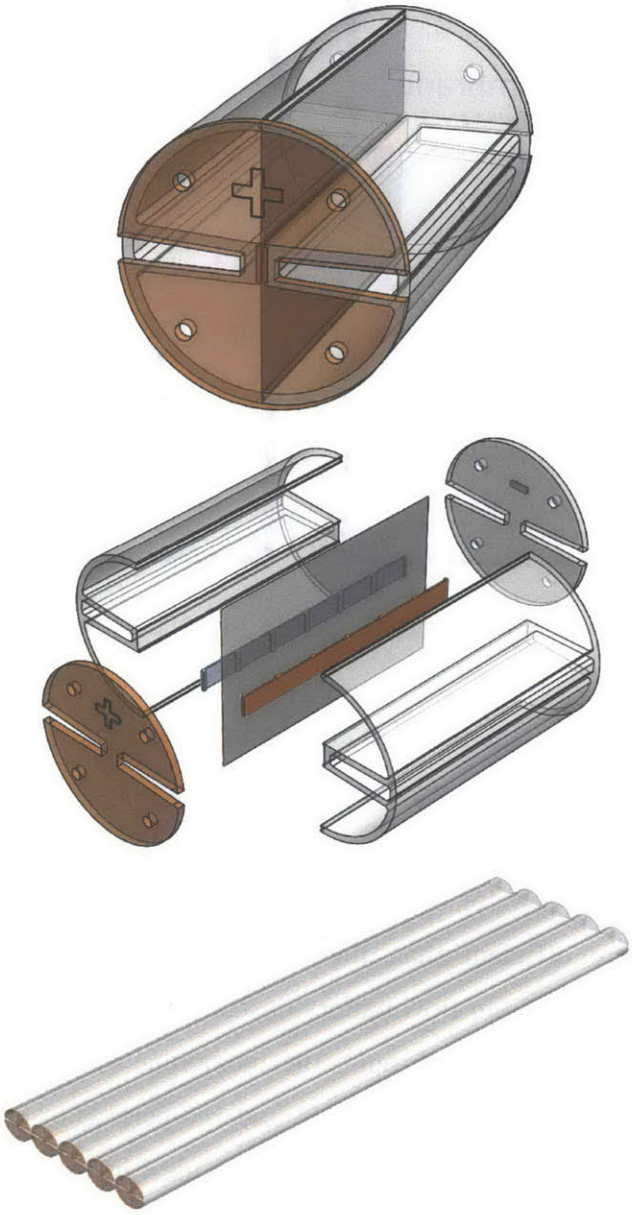

Figure 3.4: Roller-Over Flow Battery Structure

The roller-over flow battery is an option that eliminates the triangular stand in Figure 3.2. If the fluid cannot flow quickly enough by gravity alone, weights to push the fluid could be added.

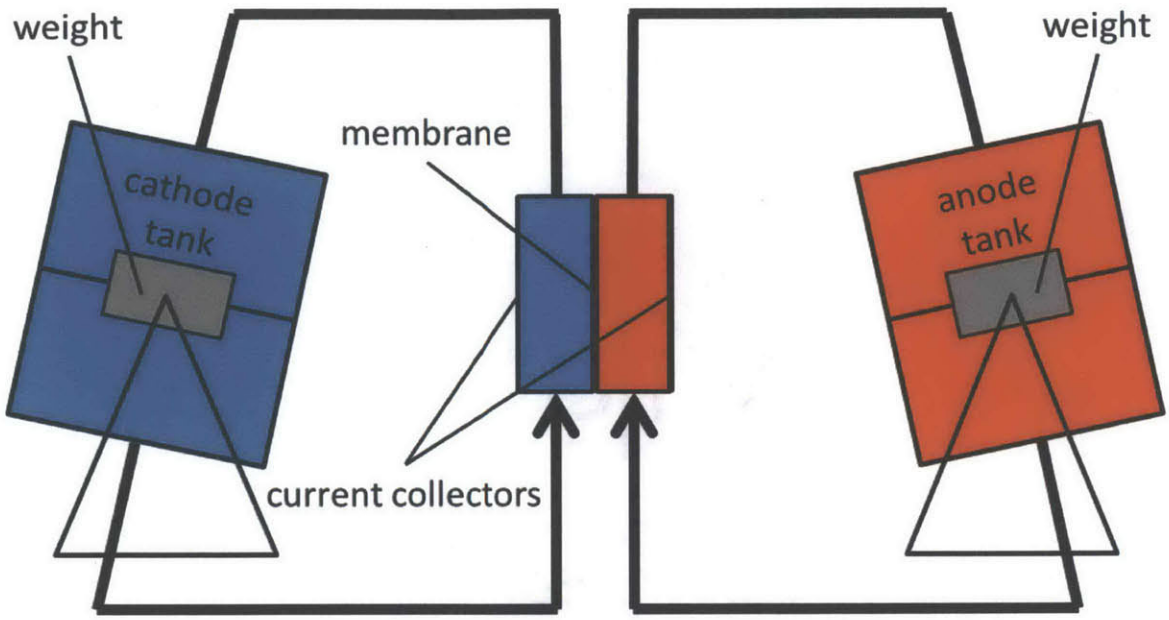

Figure 3.5: Pressurized Gravity Induced Flow Battery

In this design, flow is driven by the pressure created by weights pushing down on the anode and cathode fluid in storage tanks. The weights connected to a sealed-separating plate can freely move inside the tanks and can be tipped on pivots that are connected to the outside of the tank. Tipping the weights would allow for flow control. These designs, however, do not have a high likelihood of being more efficient than the conventional design. Centrifugal pumps are frequently used in current vanadium flow battery designs and run at low torque and high speeds. When the fluid must be recirculated through the membrane and current collector region, the motors in the gravity induced flow battery would undergo periods of high torque and low speed potentially requiring more expensive motors than those used in the pumps for the conventional design. Even if pumping efficiency gains were made with the gravity induced flow battery design, the relative gain would be small as the approximately 50% efficient centrifugal pumps only account for less than 3% of the overall energetic efficiency.

3.3 Suspension-Based Flow Battery Prior Art

The prior art associated with suspension-based flow batteries and other flow batteries share common design features that include various pumps and valves that regulate the flow of anode and cathode fluids into and/or out of a chamber at which an electrochemical interaction occurs

across a membrane that separates the anode and cathode fluids. Figure 3.6 shows a diagram of a suspension-based flow battery [16]. Items 275 and 265 are pumps. The separator membrane is item 210, and item 270 and 260 are the tanks that hold the anode and cathode fluid.

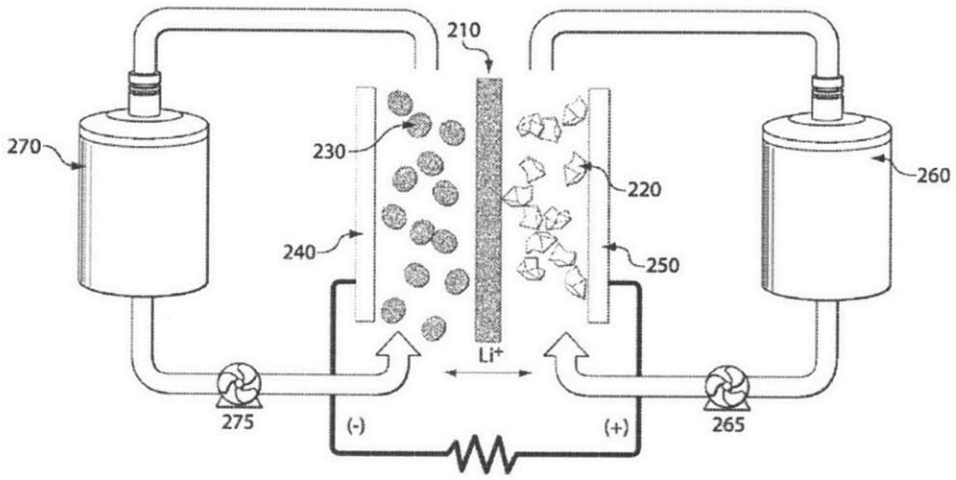

Figure 3.6: Diagram of Suspension-Based Flow Battery [17]

In Figure 3.6, items 230 and 220 represent the semi-solid fluid. One fluid is a lithium-ion source, and the other fluid is a lithium-ion sink. The membrane, item 210, only allows lithium across. As the lithium ions transfer from one side to the other, electrons are transferred to plates, items 240 and 250, which are connected by a wire with load on it. The electrons travel from one side to the other through the load to keep the two sides of the system electrically neutral. Once the anode and cathode fluid have passed by the separator membrane, they are discharged and can no longer be used as a source of energy until they are recharged. This discharged fluid travels back to a different compartment in the tanks from which they come.

One major difference between suspension-based flow batteries and other flow batteries is that anode and cathode material is shear-thinning and has a yield-stress. In order to overcome the difficulties of moving the non-Newtonian fluid through the system, Chiang provides a variety of solutions shown in Figure 3.7. Figure 3.7 a) presents a conveyor belt that pushes the fluid through the separator membrane area. Figure 3.7 b) shows an auger pushing fluid through circular separator membrane geometry. Figure 3.7 c) portrays a gas or a non-viscous fluid being pumped into the fluid stream to facilitate flow.

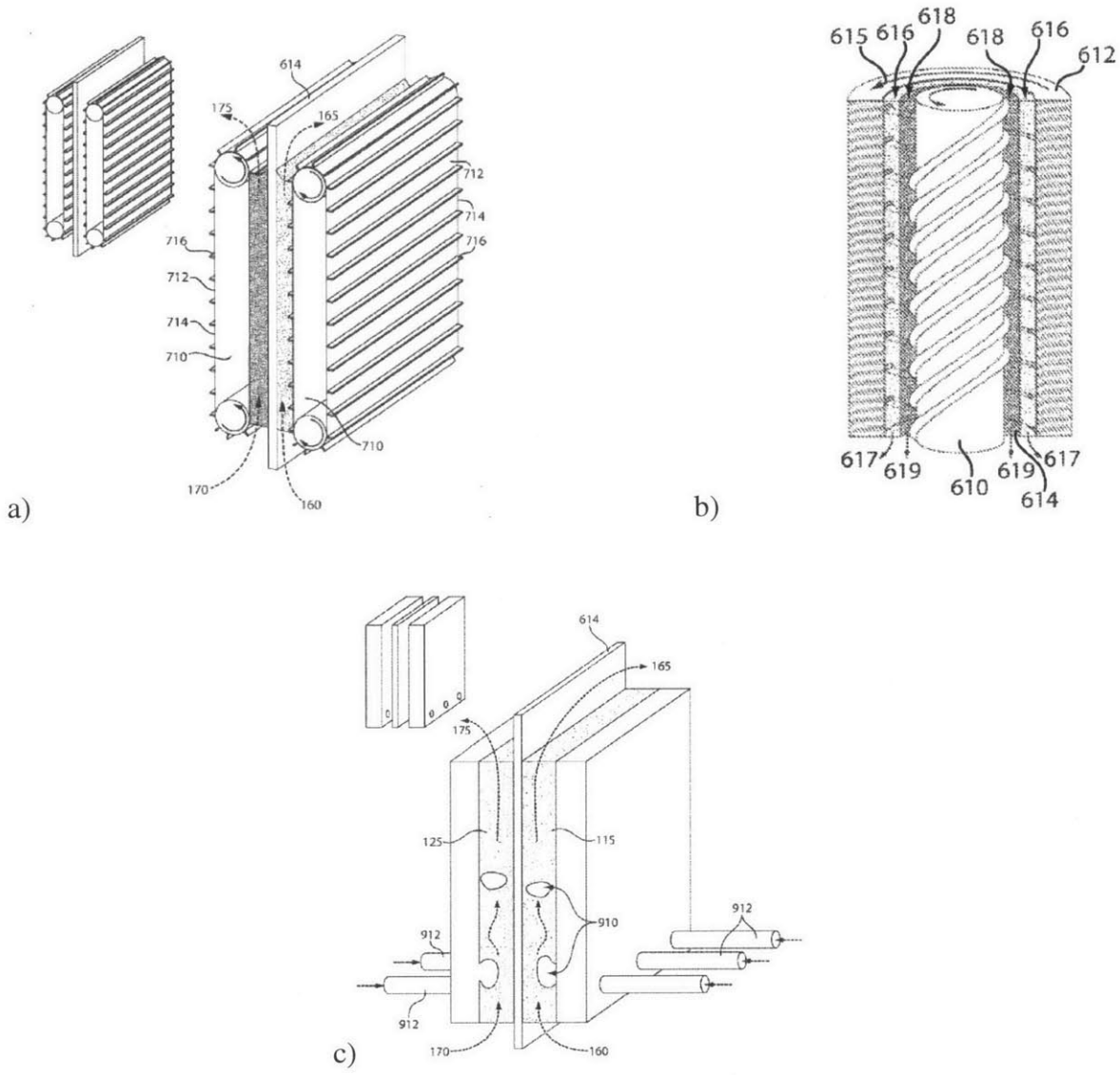

Figure 3.7: Methods to Improve Flow in Suspension-Based Flow Batteries [17]

Another unique issue with the suspension-based flow battery is that the separator membrane is not rigid and bows between the plates as the two anode and cathode material move across its sides. Other flow batteries require carbon felt between the membrane and current collector that supports the separator membrane. Chiang presents one solution, shown in Figure 3.8 to keep the membrane equally spaced between the rigid conducting plates involving pegs that protrude from the plates to hold the membrane in place.

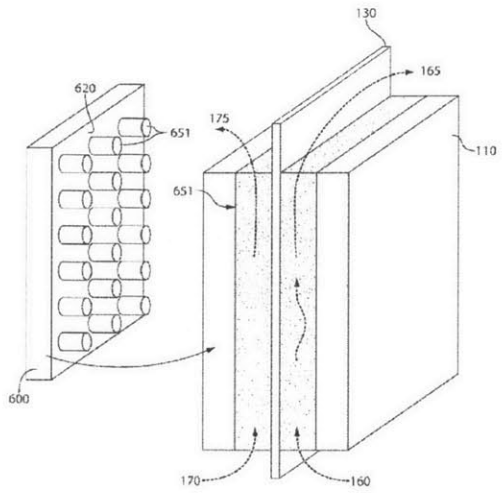

Figure 3.8: Method to Improve Membrane Stability in Suspension-Based Flow Battery [16]

3.4 Design Requirements

There are two principle design requirements for the battery.

1. **Cost per unit energy is less than or equal to $100/kWh.**
2. **Energetic efficiency is greater than or equal to 95%.**

Section 2.2 outlines that there are, however, a minimum of ten variables that affect the achievement of these two design requirements. The next design requirements presented are factors that affect the cost per unit energy and energetic efficiency.

3. **Channels in the flow battery remain clog free.**

The anode and cathode materials can easily clog in a channel that has a small cross-sectional area. If the anode and cathode material is unable to flow, the battery cannot properly store or release its full energy potential. Clogged channels can also cause pressure build up that leads to membrane rupture, which shorts the battery.

4. **Membrane is free of holes larger than the standard pore size.**

Anode and cathode material can have different viscosities that require different pumping pressures to maintain equal flow rates on the anode and cathode sides. Differences in pressure

between the anode and cathode side of a cell can cause the membrane to plastically deform or rupture, which would short the battery.

5. Ions only diffuse across the membrane.

When a plug of anode and cathode material in between the membrane and current collectors is charged or discharged, ions pass through the membrane and electrons move to and go out of the current collectors. Material in tanks above or below this electrochemically active zone, or EAZ, will be deficient or rich in ions that are rich or deficient in the EAZ. The EAZ causes gradients that induce diffusion. Diffusion of different species of ions on the anode or cathode side, not across the membrane, causes a decrease in efficiency because the electrical potential drops as the ions diffuse.

6. Volumes of anode and cathode material only spend sufficient time in the EAZ to be either fully charged or discharged.

When a charged or discharged plug is pumped out of the EAZ region a significant portion of the anode and cathode material is still in the EAZ and takes on a crescent shape due to the no-slip boundary condition as shown in Figure 3.9. Material stuck to the sides of the EAZ region can be charged or discharged for an unnecessarily long time leading to decreases in efficiency and increases in cost.

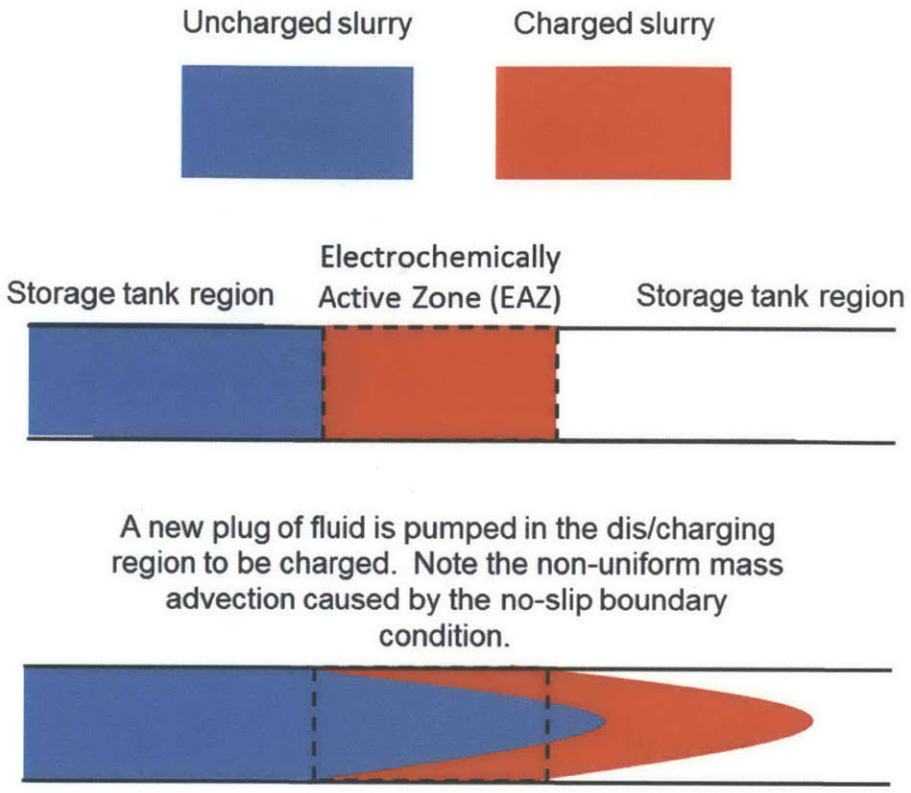

Figure 3.9: Anode or Cathode Material Sticking to Walls of EAZ

3.5 Chapter Overview

This section investigates the mechanical design of suspension-based flow batteries. The mechanical design of conventional flow batteries is presented for comparison. New concepts for conventional flow battery architectures are outlined. Such new concepts, however, would probably not provide a significant improvement in cost or efficiency in comparison to the existing flow battery design. Prior art and design requirements for suspension-based flow batteries are specified.

Chapter 4

Prototype I: Membrane Testing

4.1 Chapter Overview

The purpose of Prototype I was to demonstrate that a suspension-based flow battery could run over an extended period of time without membrane rupture. If the membrane can only withstand a small number of plug cycles without rupturing, the battery will fail regardless of how energy dense the anode and cathode materials are. Key points for designing an EAZ that avoids membrane rupture are (*i*) having channels with sufficiently large cross-sectional areas, and (*ii*) properly supporting the membrane either by carefully selecting membrane shapes or by having corrugated current collectors directly touch the membrane. Prototype I clarified how to properly meet Design Requirements 3 and 4.

4.2 Design Strategies

The following strategies are options to support the membrane sufficiently so that when there is a pressure differential across the membrane, plastic yielding will not occur. Anode and cathode viscosity can vary depending on the type of materials used, so the strategies presented are guides to help in the design process that can be adapted to the specific anode and cathode materials' needs.

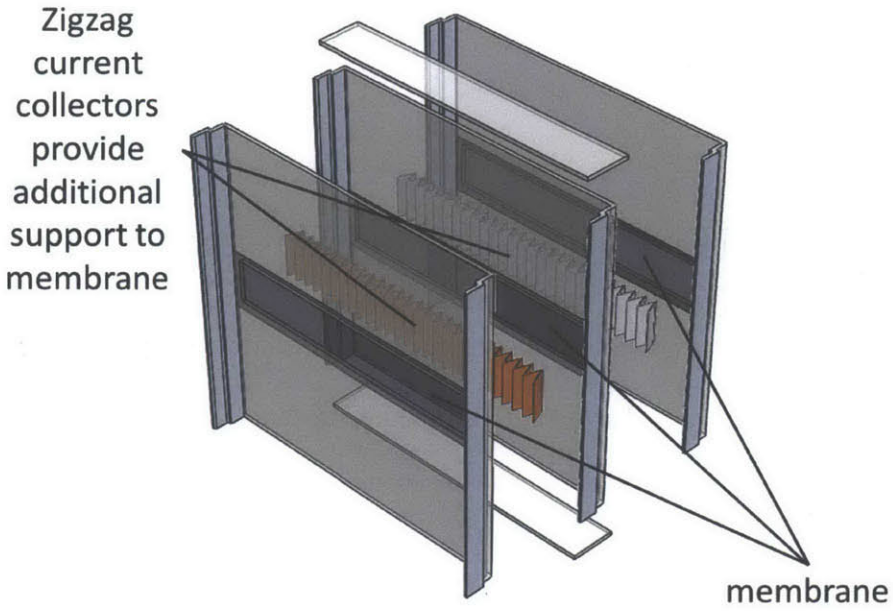

Figure 4.1: CAD Model of Single Cell in Stack

1. Boundary Support

The membrane shown in Figure 4.1 is heat sealed to the structural casing on all four sides. The maximum deflection and stress of the membrane can be approximated using the following equations from *Roark's Formulas for Stress and Strain* [18].

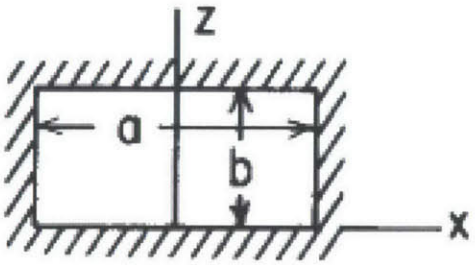

Figure 4.2: Rectangular Membrane with All Fixed Edges

$$y_{max} = \frac{\alpha q b^4}{E t^3} \tag{4.1}$$

$$\sigma_{max} = \frac{\beta q b^2}{t^2} \tag{4.2}$$

a/b	1.0	1.2	1.4	1.6	1.8	2.0	∞
α	0.0138	0.0188	0.0226	0.0251	0.0267	0.0277	0.0284
β	0.3078	0.3834	0.4356	0.4680	0.4872	0.4974	0.5000

Table 4.1: Values of Constants

a = [m] long dimension of membrane

b = [m] short dimension of membrane

y_{max} = [m] maximum deflection of membrane

α = [-] variable associated with the dimensions of the membrane

q = [Pa] pressure differential across the membrane

b = [m] shortest dimension of membrane, not thickness of the membrane

t = [m] thickness of membrane

β = [-] variable associated with the dimensions of the membrane

This strategy covers the lease amount of membrane and minimizes the pressure required to pump the anode and cathode materials past the EAZ.

2. Laminated Support

Another method to support the membrane is to laminate the membrane between two thin polymer sheets as shown in Figure 4.3.

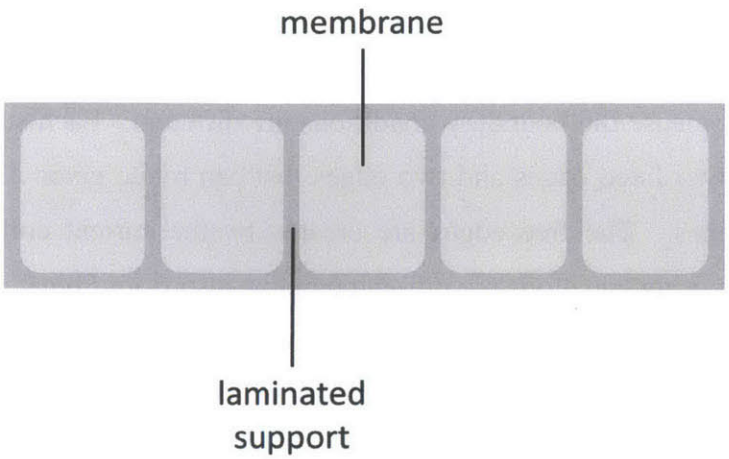

Figure 4.3: Laminated Membrane Support

The same equations and analysis shown in the Boundary Support section and can be used for this strategy as well only now a and b are the dimensions of the windows created by the laminated support. The window shapes need not be rectangular but could also be shaped like squares, circles, or rhombuses for example. This strategy covers up more of the membrane than the Boundary Support strategy and does not necessarily provide more support. If the smallest supported dimension of the membrane is equal using both strategies, the maximum stress in the membrane can be approximately equal for a constant pressure gradient.

3. Corrugated Current Collector Support

The membrane can also be supported by a corrugated current collector as shown in Figure 4.1. The support from the current collector could take on many shapes as shown in Figure 4.4.

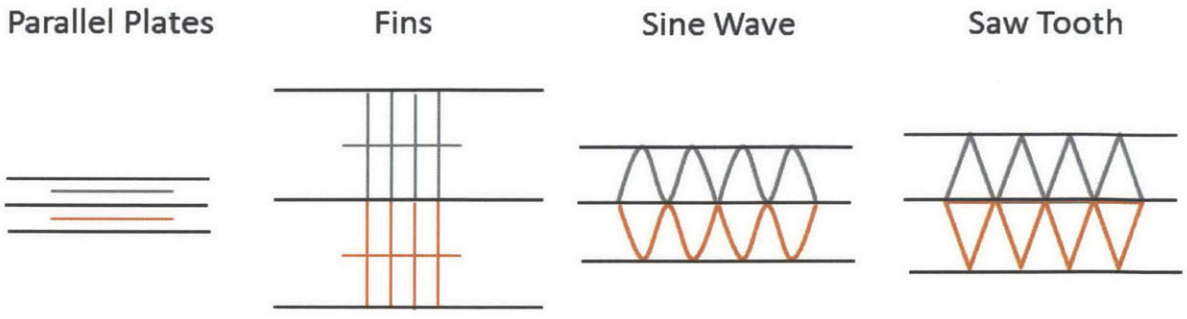

Figure 4.4: Current Collector Support Options, direction of flow is into the page

The analysis used to assess these options is different than that used in the Boundary or Laminated Support because the boundary conditions are different. Each supported piece of the membrane now has two fixed edges and two edges that can rotate given a moment, also called simply supported edges. The free edges are created by the current collector contacting the membrane. The governing equations are presented below also from *Roark's Formulas for Stress and Strain* [18]. This method increases the amount of pressure required to pump the anode and cathode materials through the EAZ and does not necessarily decrease the amount of maximum stress in the membrane better than the other presented strategies.

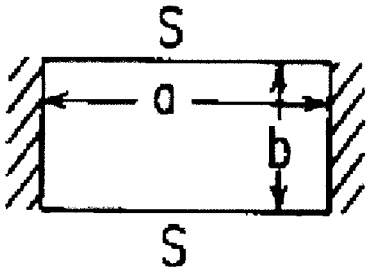

Figure 4.5: Rectangular Membrane with Two Fixed Edges and Two Simply Supported Edges

$$y_{max} = \frac{\alpha q b^4}{E t^3} \tag{4.3}$$

$$\sigma_{max} = \frac{\beta q b^2}{t^2} \tag{4.4}$$

a/b	1.0	1.2	1.4	1.6	1.8	2.0	∞
α	0.0210	0.0349	0.0502	0.0658	0.0800	0.0922	
β	0.4182	0.5208	0.5988	0.6540	0.6912	0.7146	0.750

Table 4.2: Values of Constants

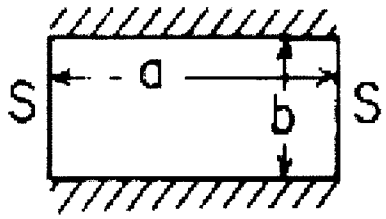

Figure 4.6: Rectangular Membrane with Two Fixed Edges and Two Simply Supported Edges

For the orientation show in Figure 4.6, the same equations are used for the orientation shown in Figure 4.5. The tabulated values, however, are different.

a/b	1.0	1.2	1.4	1.6	1.8	2.0	∞
α	0.0210	0.0243	0.0262	0.0273	0.0280	0.0283	0.0284
β	0.4182	0.4626	0.4860	0.4968	0.4971	0.4973	0.500

Table 4.3: Values of Constants

4.3 Detailed Design

Prototype I was designed, fabricated, and tested by Christian Höcker [19] and Brandon Hopkins. The purpose of Prototype I was to demonstrate that a suspension-based flow battery could run over an extended period of time without membrane rupture.

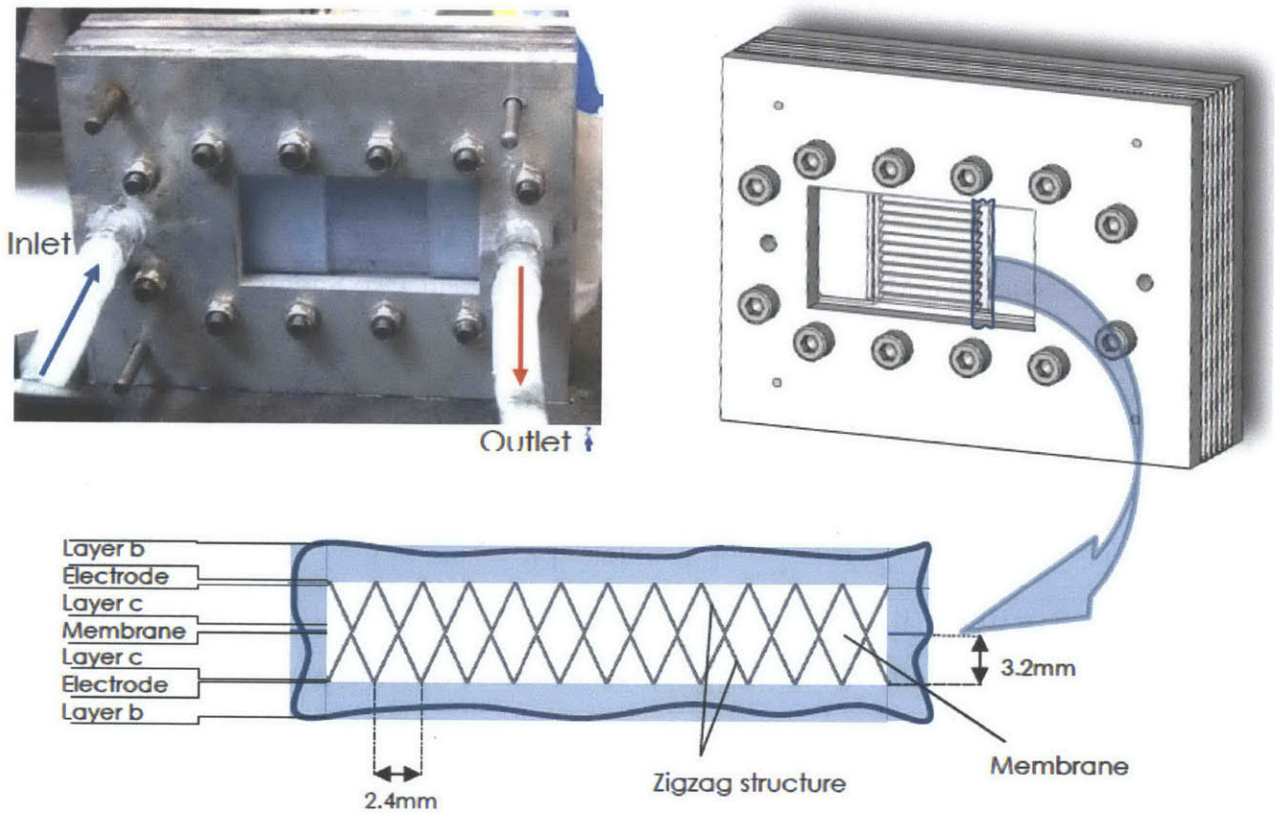

Figure 4.7: Prototype I, device top left, solid model top right, schematic of EAZ bottom

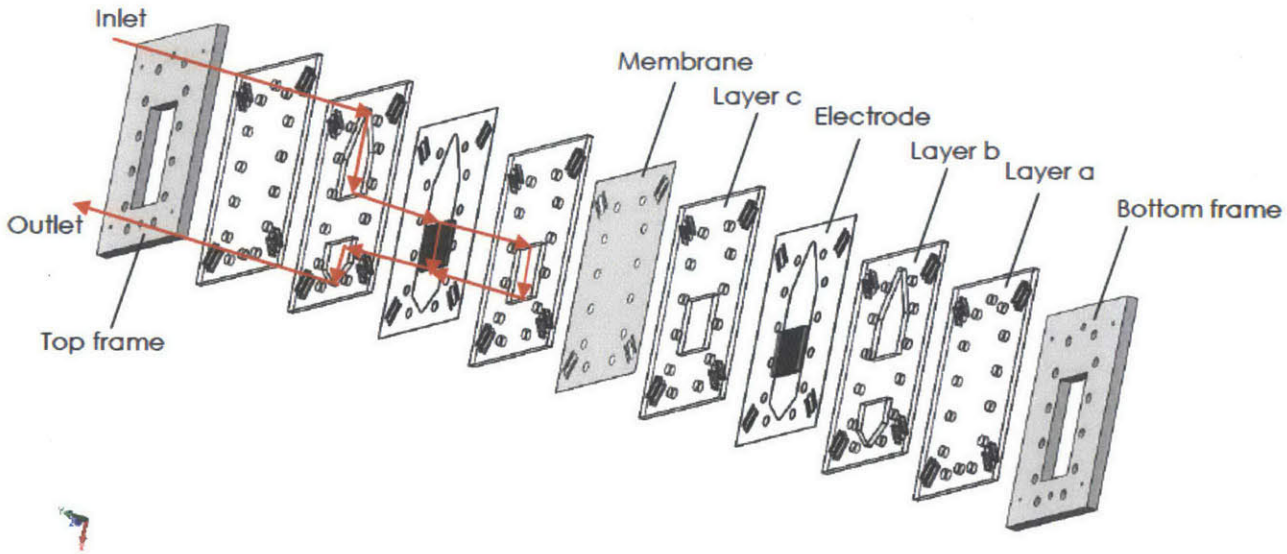

Figure 4.8: Exploded View of Prototype I, red arrows showing flow path

For this prototype, the saw tooth or zigzag current collector structure was chosen to perform flow tests using phantom fluids. The prototype was made of polycarbonate and aluminum sheet stock that was cut with a water jet. Flexures were used to act as compliant holes for positioning pins to pass through to ease battery assembly.

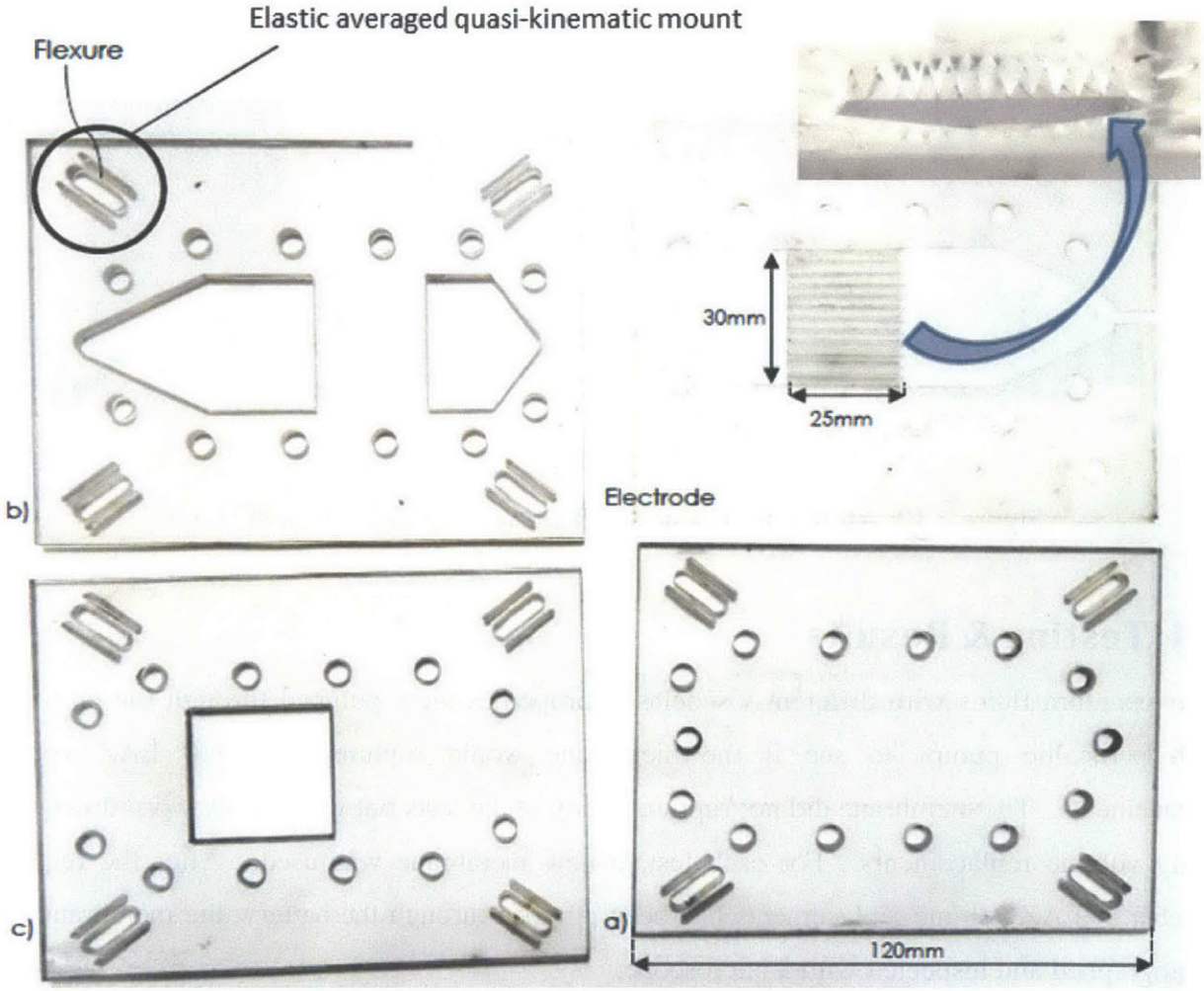

Figure 4.9: Different Layers of Prototype I

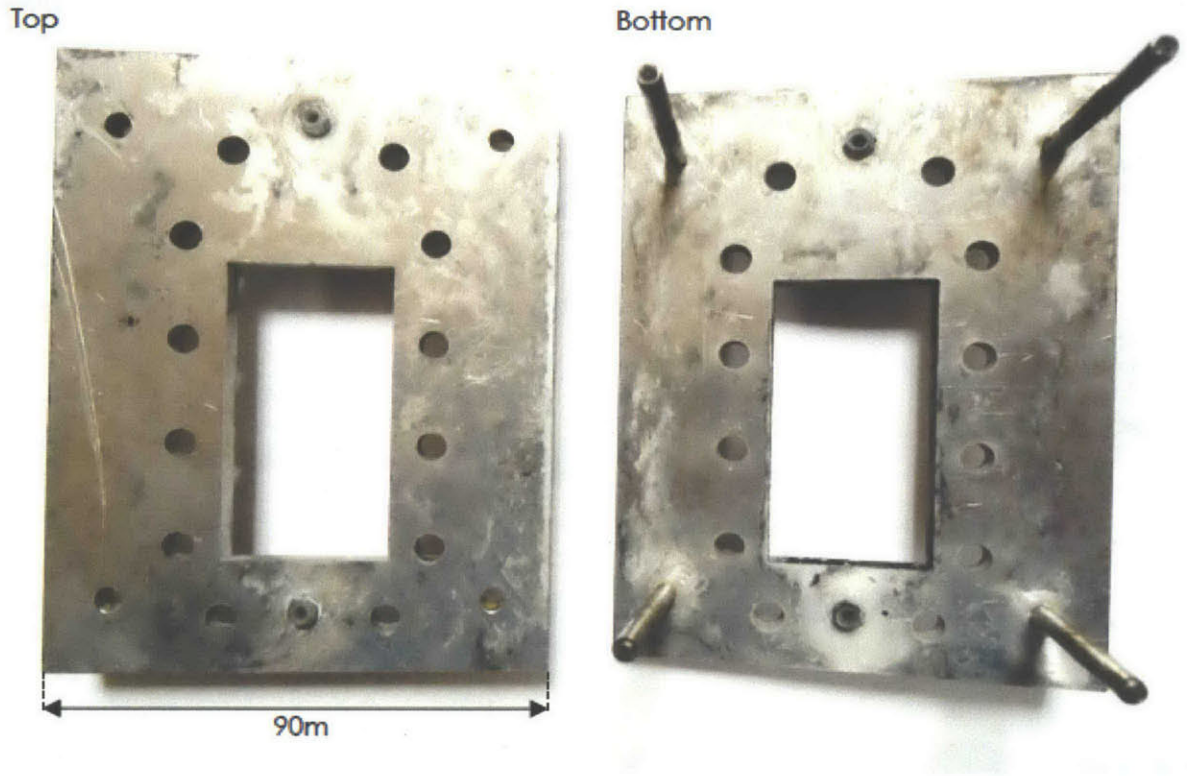

Figure 4.10: Aluminum Frames with Dowel Pins and Through Holes

4.4 Testing & Results

Four phantom fluids with different viscoelastic properties were pumped through the prototype with peristaltic pumps to see if the membrane would rupture after 500 EAZ volume replacements. The membrane did not rupture in any of the tests but was visibly worn down after many volume replacements. For each test, a new membrane was used. After the required number of EAZ volume replacements had been pumped through the battery, the membrane was photographed and inspected with a microscope.

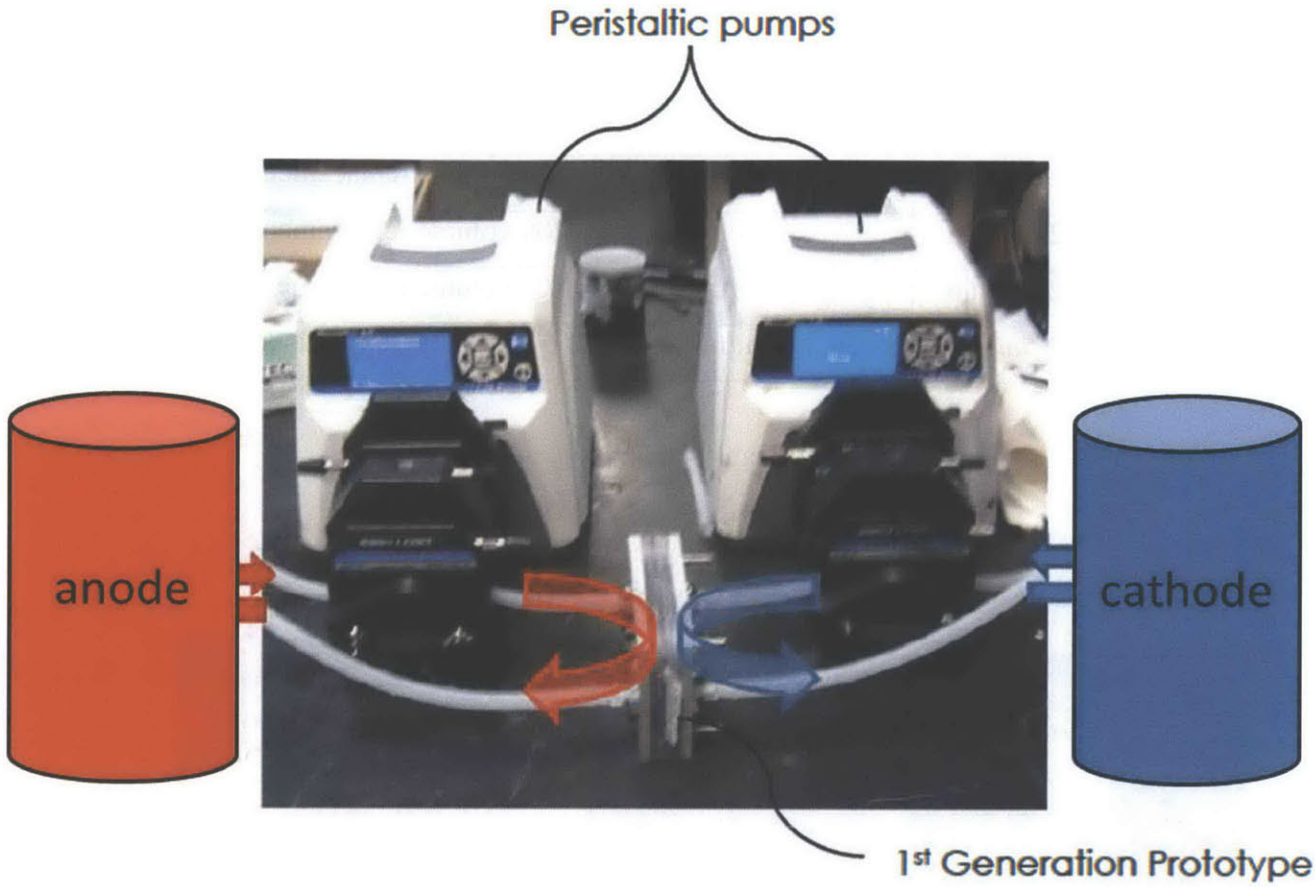

Figure 4.11: Experimental Setup

Fluid 1, F1	Neutrogena Deep Clean Facial Scrub, shear thinning material with abrasives
Fluid 2, F2	Toothpaste with no abrasives
Fluid 3, F3	Water
Fluid 4, F4	10 vol% LFP, 1 vol% Carbon black, 1 M $LiNO_3$

Table 4.4: Phantom Fluids

Test	Anode side	Cathode side	Result
1	F3, 1720 ml/min	F3 1720 ml/min	22,222 volume replacements F3, no rupture
2	F3, 1720 ml/min	F1, 15 ml/min	200 volume replacements F1, no rupture
3	F3, 1720 ml/min	F2, 32 ml/min	426 volume replacements F2, no rupture
4	F2, 32 ml/min	F1, 15 ml/min	200 volume replacements F1, no rupture
5	F2, 32 ml/min	F4, 10 ml/min	100 volume replacements F4, no rupture
6	F2, 32 ml/min	F4, 10 ml/min	1600 volume replacements F4, no rupture

Table 4.5: Test Results

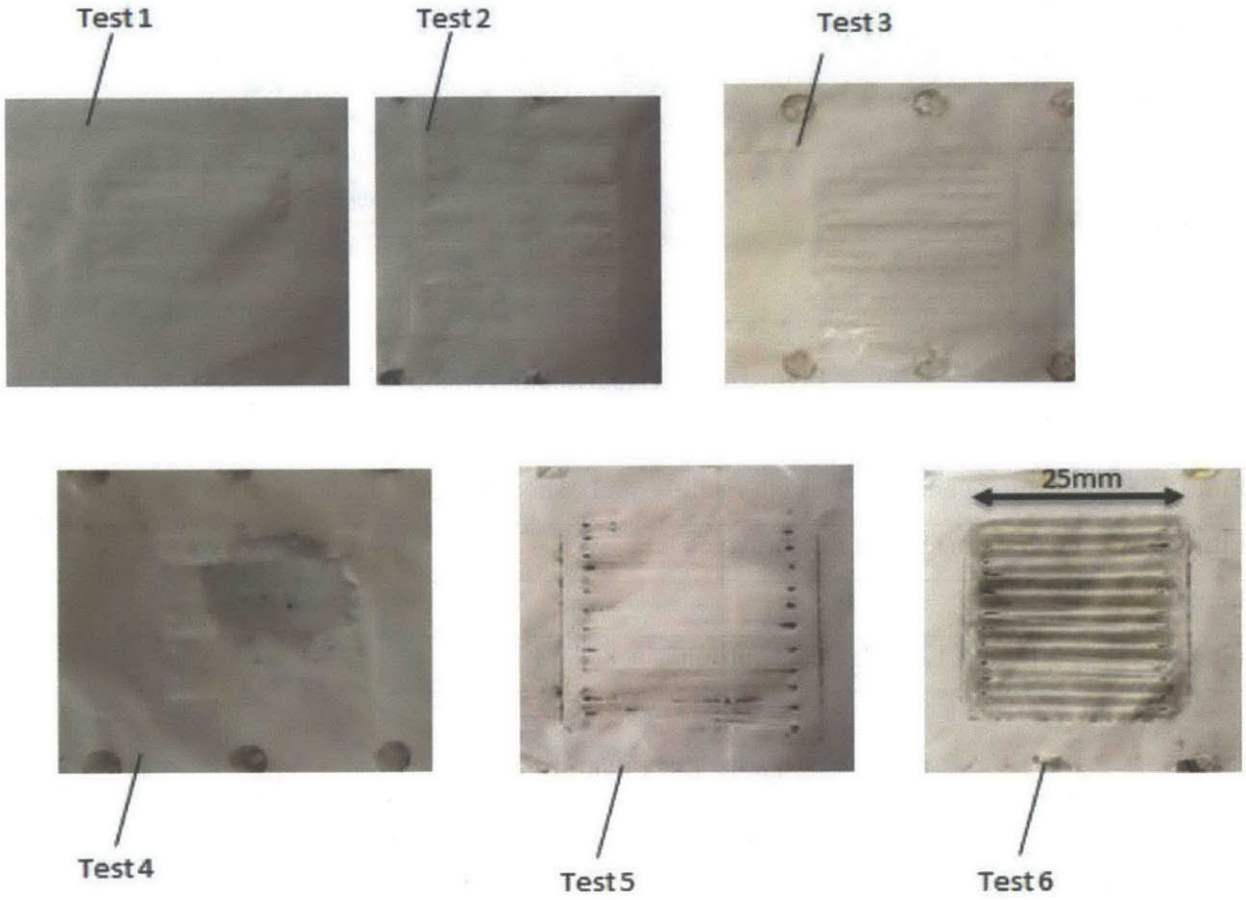

Figure 4.12: Membrane after Tests, notice the creases caused by the corrugated current collector

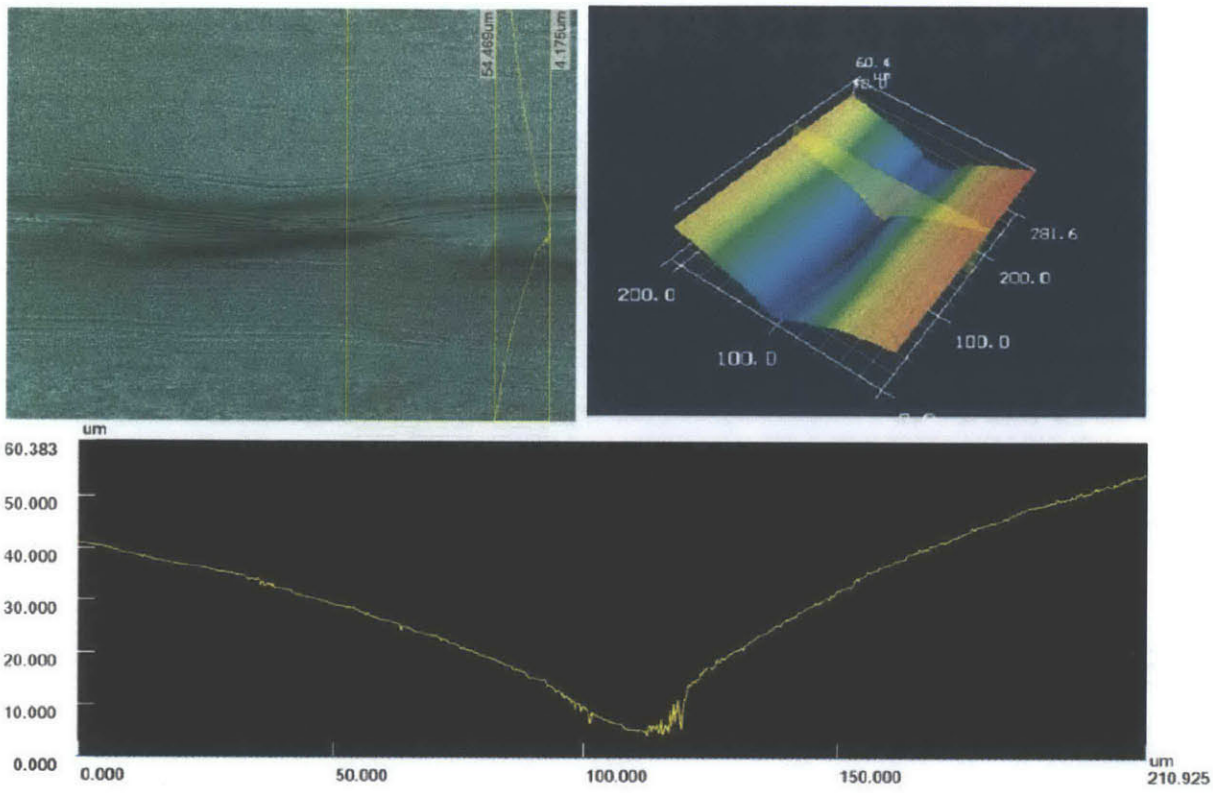

Figure 4.13: Example of Microscope Image of Dent in Membrane on Corrugation Line

4.5 Chapter Summary

The purpose of Prototype I was to demonstrate that a suspension-based flow battery could run over an extended period of time without membrane rupture. If the membrane can only withstand a small number of plug cycles without rupturing, the battery will fail regardless of how energy dense the anode and cathode materials are. Key points for designing an EAZ that avoids membrane rupture are (*i*) having channels with sufficiently large cross-sectional areas, and (*ii*) properly supporting the membrane either by carefully selecting membrane shapes or by having corrugated current collectors directly touch the membrane. Prototype I clarified how to properly meet Design Requirements 3 and 4.

Chapter 5

Prototype II: Electrochemical Testing

5.1 Chapter Overview

The purpose of Prototype II and its iteration was to demonstrate that an electrochemically functional suspension-based flow battery could be constructed and to understand how to improve energetic efficiency. Key points for designing a high energetic-efficiency battery are (*i*) the EAZ should be ideally electrically insulated from the storage tank regions, and (*ii*) the volumes of anode and cathode material should ideally travel through the EAZ with a flat velocity profile. This series of prototypes highlighted the necessity of Design Requirements 5 and 6 to achieve high energy efficiencies and led to the idea of a plug isolator mechanism in the flow battery design.

5.2 Design Strategies

The following strategies are options to electrically insulate the EAZ from the storage tanks. Conventional redox flow batteries have the same problem as described in Design Requirement 5 and the same solutions can be adapted to suspension-based flow batteries.

1. Valves

Using values to electrically insulate the EAZ from the storage tanks is an idea that has been patented for vanadium redox flow batteries [20]. The idea is to have a valve directly above and below where the current collectors begin in Figure 4.1. This option, however, would require long skinny rectangular values with dimensions on the order of 1 mm for one dimension and 1 m for the other. Creating a reliable rectangular seal that could be controlled to open and close with such dimensions seemed unfeasible. Granted, valves could be used if the entire EAZ was separated from the storage tanks by pipes just as conventional flow batteries are.

2. Increase Electrical Resistance

Increasing the electrical or ionic resistance between the tubing that connects the EAZ to the storage tank has been investigated since the creation of the first flow batteries in the 1970s [21]. The idea behind this strategy is that if a perfect sealing valve is not possible, perhaps a valve with a small leak will increase the resistance sufficiently to obtain desired energetic efficiencies. One way to increase the electrical resistance is to make obstructions immediately surrounding the EAZ as shown in Figure 5.1.

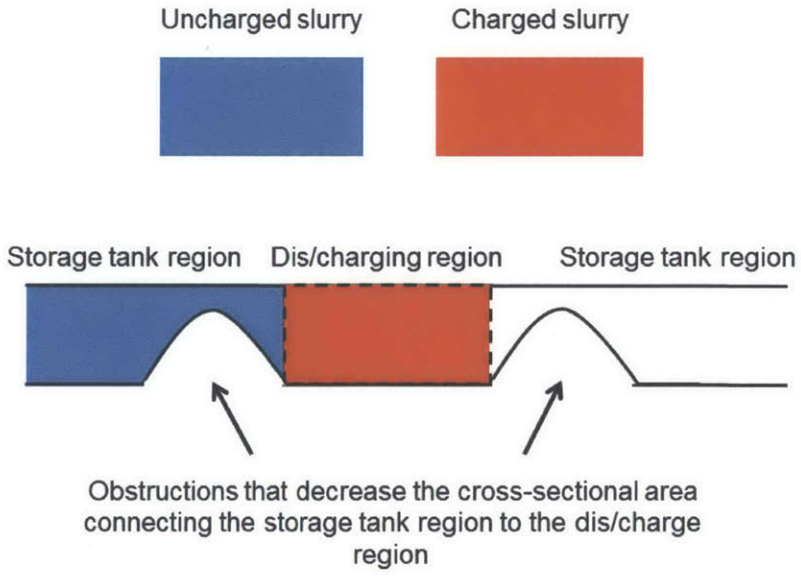

Figure 5.1: Strategy to Minimize EAZ Extension

The equation for electrical resistance is show below.

$$R = \frac{\rho l}{A} \tag{5.1}$$

R = [Ω] electrical resistance

ρ = [Ω*m] electrical resistivity

l = [m] length of electrically conductive material

A = [m^2] cross sectional area of electrically conductive material

This strategy suggests decreasing A to increase R. However, as A decreases, not only does the electrical resistance increase but also the fluidic resistance increase requiring a larger pump to move the anode and cathode material through the EAZ.

3. Plug Isolator Mechanism

The idea of using a plug isolator mechanism came by realizing the need for Design Requirement 6. Two possible plug isolator mechanisms, shown in an exploded view, are displayed in Figure 5.2 and 5.3.

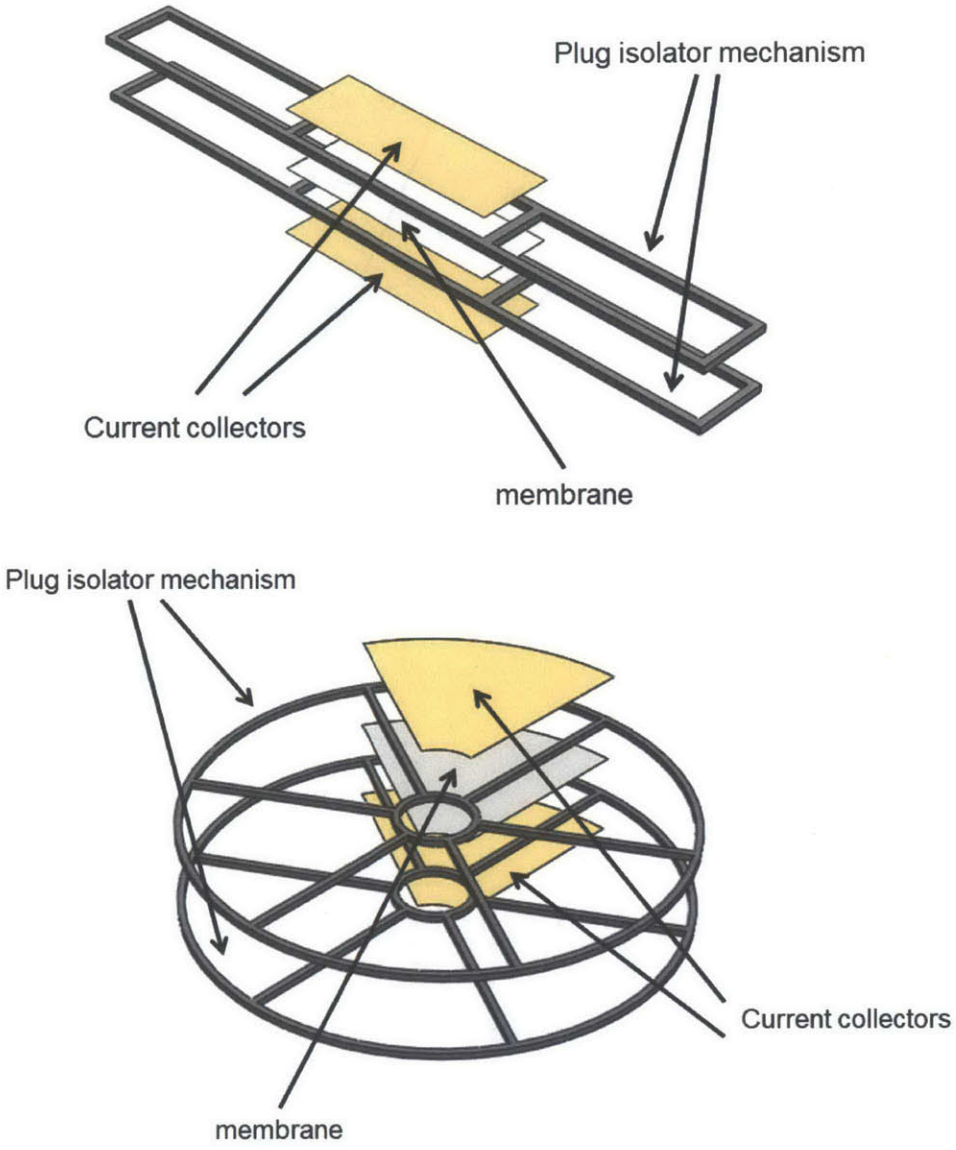

Figure 5.2: Linear and Rotary Version of Plug Insulator Mechanism

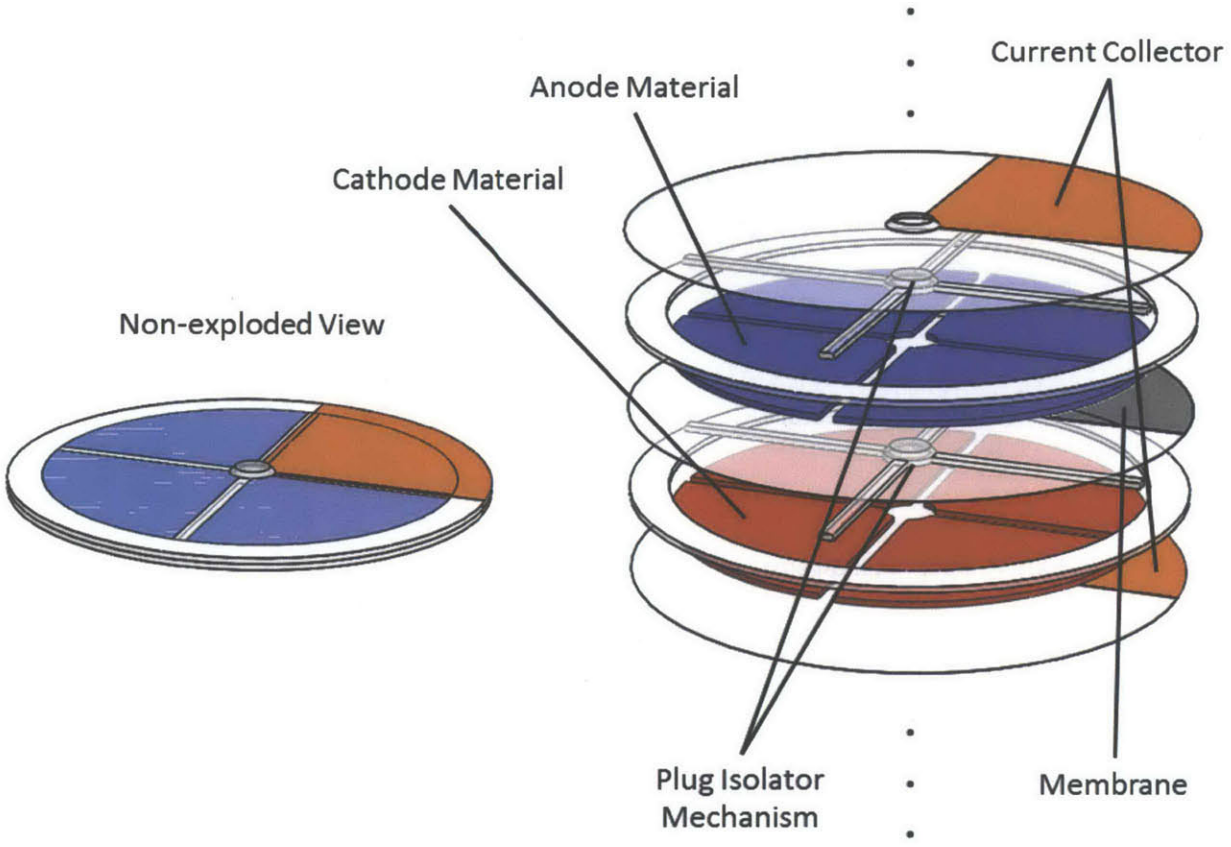

Figure 5.3: Detailed Design of Rotary Plug Isolator Battery

A plug isolator would be a mechanical obstruction that would physically isolate each plug of the flow battery. Instead of controlling the flow of the system pumps, the anode and cathode material would be pushed by the plug isolator mechanism that would be controlled by a motor. The plug isolator would nearly electrically isolate each plug from each other, assuming that leaks in the seals are small, and would enforce a flat velocity profile at the front and back of each plug thus satisfying Design Requirement 6. The plug isolator would scrape the EAZ clean whenever a new plug was moved in. A plug isolator, however, adds inactive material to the battery that could increase the cost per unit energy. Jamming of the plug isolator is also a risk associated with this strategy.

5.3 Detailed Design

Prototype II was designed, fabricated, and built by Brandon Hopkins and Christian Höcker. The purpose of this prototype was to demonstrate the feasibility of constructing an electrochemically functional suspension-based flow battery and to understand how to improve energetic efficiency. Most of the prototype was 3D printed using Somos 11122 material. Outer aluminum plates were cut with a water jet. The current collector region was created by sputtering gold onto the 3D printed plastic.

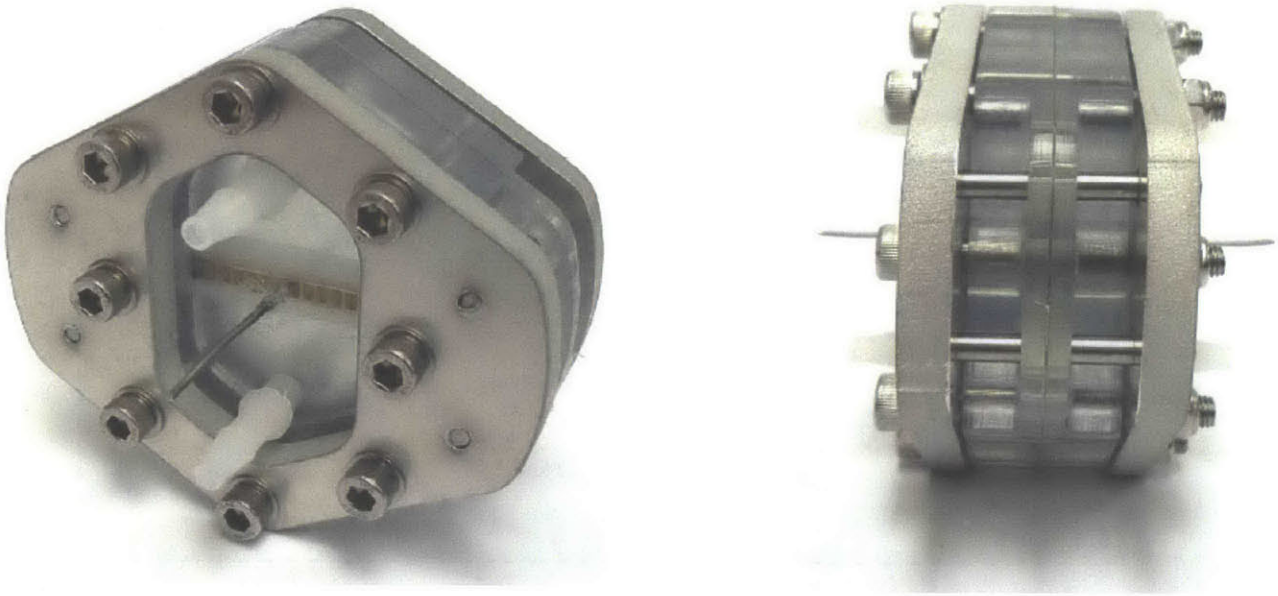

Figure 5.4: Prototype II

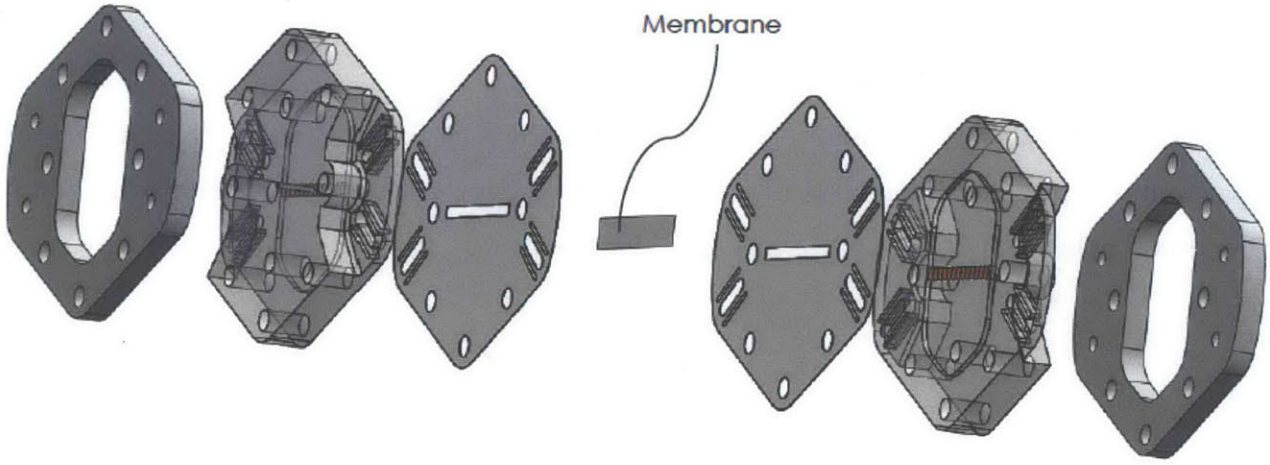

Figure 5.5: Exploded View of Prototype II CAD Model

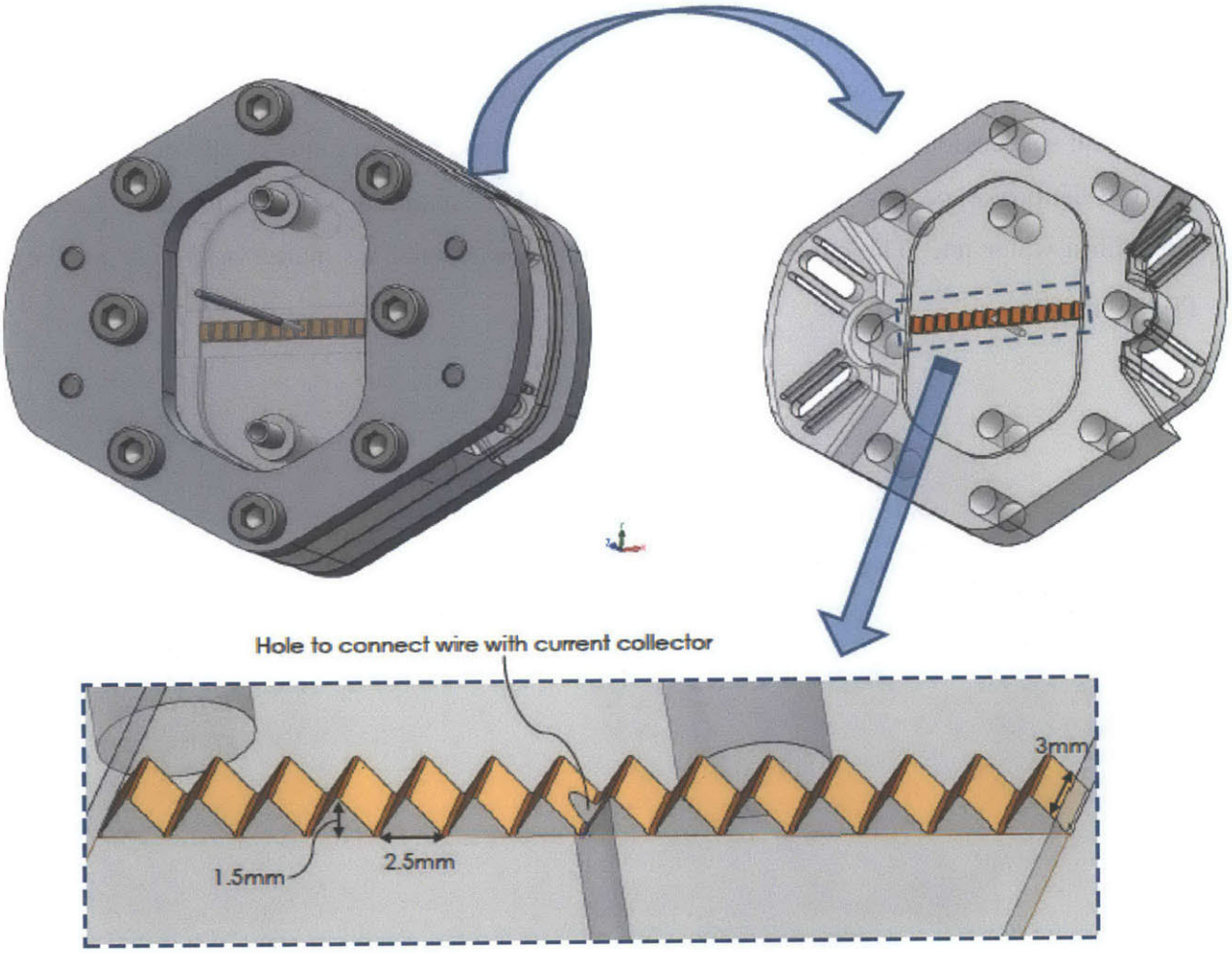

Figure 5.6: CAD Model Detail of Prototype II Showing Corrugated Current Collector

5.4 Testing & Results

Aqueous 10 vol% LFP/ 15 vol% LTP with 1 vol% carbon black was used as the cathode/anode pair and was pumped through the battery with syringe pumps as shown in the experimental set up shown below.

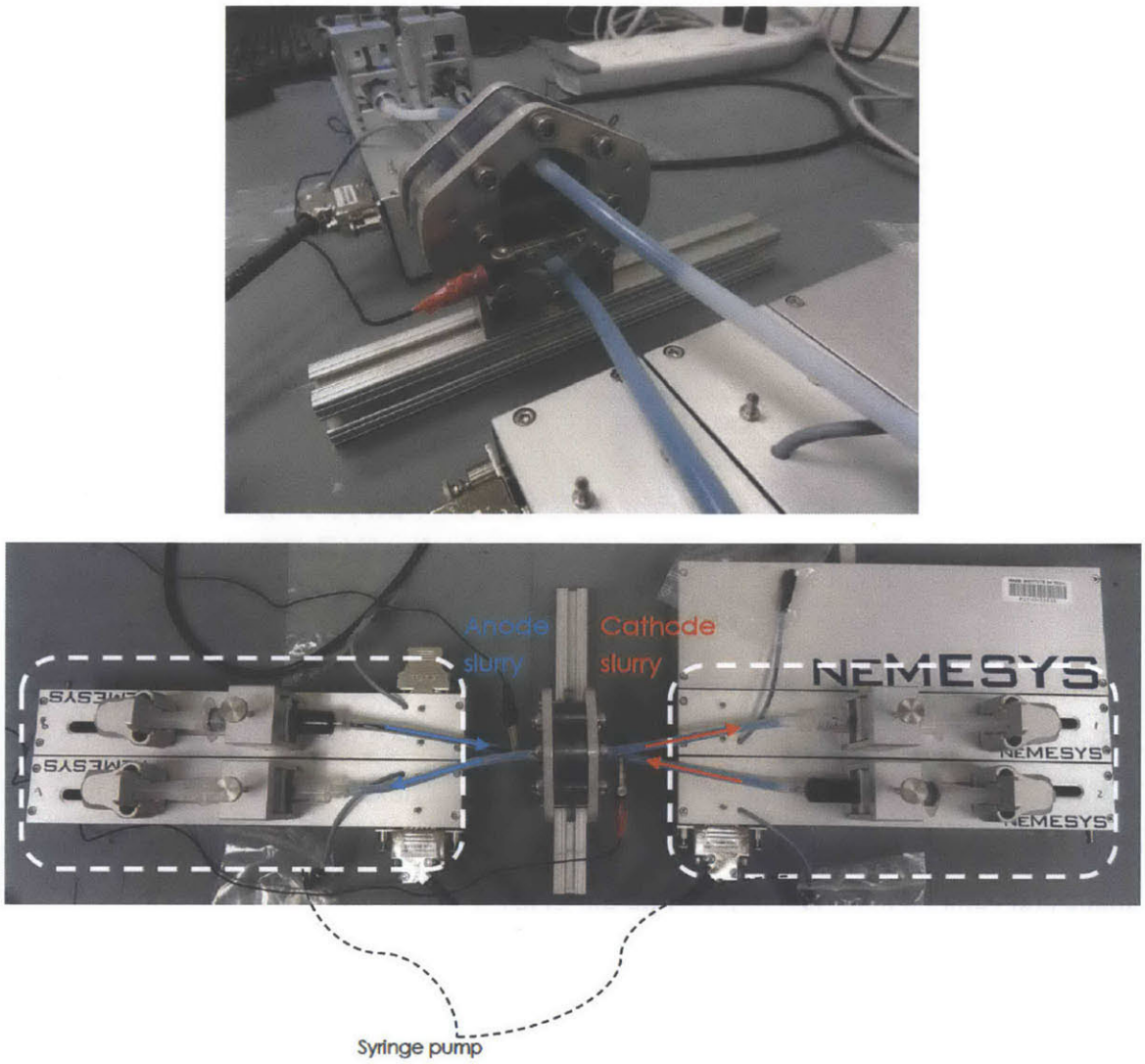

Figure 5.7: Prototype II Experimental Setup

The anode and cathode materials were charged at 0.5 mA until a potential difference of 1.1 V was achieved. To discharge the material, the material was placed under negative 0.5 mA until a potential difference of 0.5 V was achieved. The graph below summarizes the electrochemical data. The first charge-up cycle lasted for almost 40 h, which is significantly longer than the amount of time required to charge up the 0.1 ml of material in the EAZ, which was calculated to be closer to 4 h. This data shows that the EAZ was effectively extended and highlighted the need of Design Requirement 5 as the reaction was extending to the storage tanks and not being confined to the EAZ.

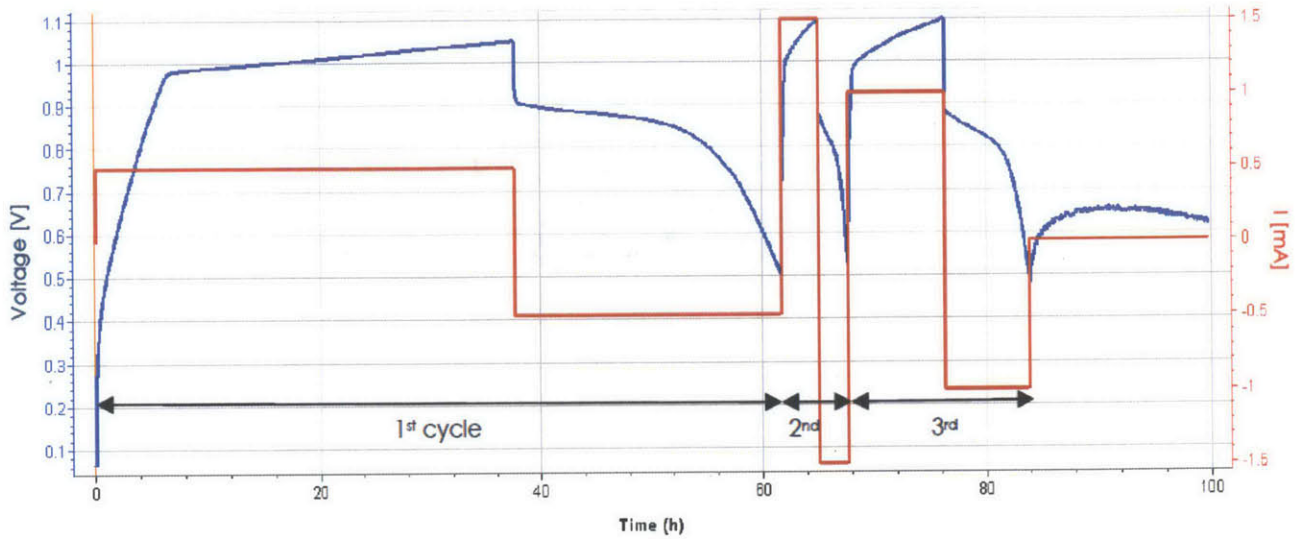

Figure 5.8: Electrochemical Data from Prototype II

In response to this data, the prototype was modified by implementing Strategy 2, increasing electrical resistance by adding a barrier. Two elastomer barriers were place above and below the EAZ of the anode and cathode side of the battery to act as a flexible seal shown in Figure 5.9 that allowed only a small gap of 0.5 mm from the peak of the zigzags to the top of the boundary for the anode and cathode materials to pass into the EAZ.

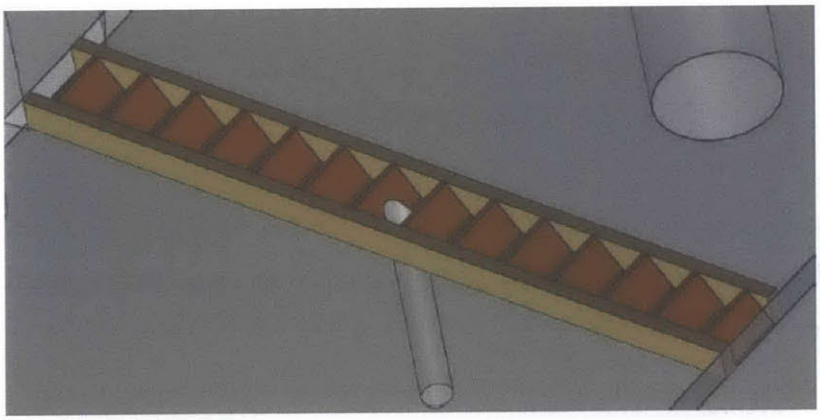

Figure 5.9 CAD Model Detail of Modified Prototype II

The electrochemical data from this modified prototype is shown in Figure 5.10. The electrical resistance between the EAZ and the storage tank appears to be higher than when there were no barriers as the charging time is now approximate 5 h instead of 40 h.

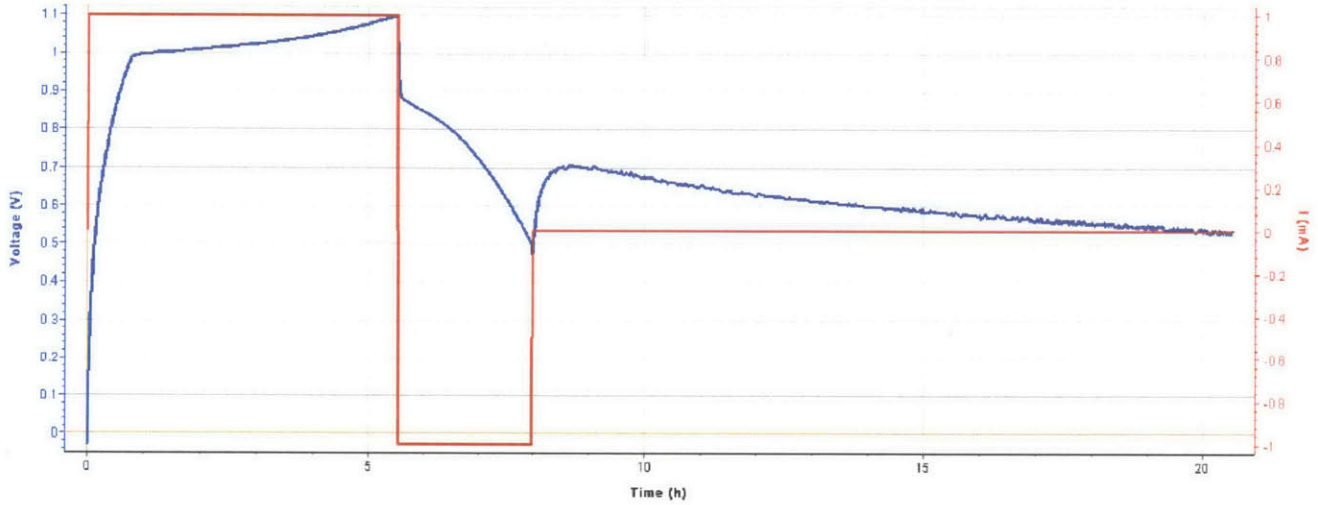

Figure 5.10: Electrochemical Data from Modified Prototype II

The fundamental problem, however, that is not solved by the prototype modification is the problem described in Design Requirement 6. If anode and cathode materials are pumped from a small slit into the EAZ when a new plug is to be charged or discharged, a significant amount of material from the old plug will have stuck to the walls and will lower the energetic efficiency of the system. Another plug of fluid was pumped into the modified prototype to test the effect of the anode and cathode material sticking to the walls, but the elastomer barriers broke off due to the pressure required to move the fluid. This event demonstrated the tradeoff between increased electrical resistance between the tank and EAZ and the increased pressure required to run the system.

5.5 Simulation Results

Kyle Smith, the electrochemical modeler on the team, created a simulation model to explore the effect of anode and cathode material sticking to the walls of the EAZ region and EAZ extension as they relate to energetic efficiency. The simulation was tested and verified using

electrochemical experiments. The details of the electrochemical model are not the focus of this thesis. Three solutions were proposed to avoid these two problems.

1. Plug Fractions

Pump only fractions of a plug at a time into the EAZ thus decreasing the extended nature of the crescent shaped flow pattern without using barriers surrounding the EAZ.

2. Pump Slowly

Pump the plugs slowly into the discharge/charge zone so that they maintain a plug-like region in which a central region of the velocity profile would be flat because the fluid is shear thinning without using barriers surrounding the EAZ.

3. Plug Isolator Mechanism

Create a plug isolating mechanism that would force the plugs to have a flat velocity profile and that electrically insulates one plug from another, essentially using moving barriers that surround the EAZ for every individual plug.

Simulations were performed to investigate these solutions as shown in Figure 5.11.

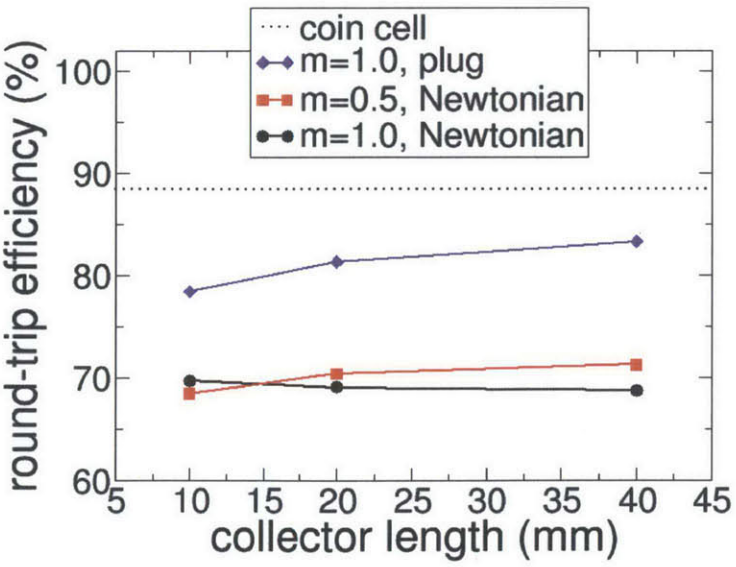

Figure 5.11 Simulation Results Demonstrating Need for a Plug-Isolator Mechanism

The "collector length" refers to the length of the EAZ in the direction of anode and cathode flow. The C rate for all trials was C/5. The round-trip energetic efficiency slightly improves with increasing EAZ length. The m = 1 Newtonian fluid means no portion of the velocity profile is flat due to the high shear rate, in which one full plug is pumped into the discharge/charge region at a time. The m = 0.5 Newtonian fluid assumes half plugs are pumped into the discharge/charge region at a time as proposed in Strategy 1. The m = 1 plug represents a fluid that has a significant flat region in the velocity profile which corresponds with Strategy 2. The dotted line represents the data for a static electrode battery where the EAZ is region is completely electrically isolated from the tank region because there is no tank region. This data could be compared to a perfectly functioning plug isolator mechanism. One of the primary design requirements is that the battery needs to have an energetic efficiency near 95%. This plot demonstrates that in order to achieve such energetic efficiencies only Strategy 3 could be acceptable. More analysis is currently being performed to identify ways to avoid the plug-isolator mechanism as it adds significant complexity to the system of the battery especially as the number of plugs increases.

5.6 Chapter Summary

The purpose of Prototype II and its iteration was to demonstrate that an electrochemically functional suspension-based flow battery could be constructed and to understand how to improve energetic efficiency. Key points for designing a high energetic-efficiency battery are (*i*) the EAZ should be ideally electrically insulated from the storage tank regions, and (*ii*) the volumes of anode and cathode material should ideally travel through the EAZ with a flat velocity profile. This series of prototypes highlighted the necessity of Design Requirements 5 and 6 to achieve high energy efficiencies and led to the idea of a plug isolator mechanism in the flow battery design. In order to achieve efficiencies near 95%, a plug isolator mechanism may be necessary.

Chapter 6

Prototype III: Flow Control

6.1 Chapter Overview

The purpose of Prototype III was to demonstrate how the flow of anode and cathode material in a suspension-based flow battery could be controlled. The method of control is dependent on the amount of pressure required to push the anode and cathode material through the battery. This section presents multiple options for a range of viscosities. Strategies that function for high viscosities also function for low viscosities.

6.2 Design Strategies

Low viscosity

1. Gravity Free Fall

Have no added pressure to move the anode and cathode material other than their own weight as shown in Figure 6.1. Weights above each individual column of anode and cathode material could also add pressure. A plug isolator mechanism could be incorporated into this method of control.

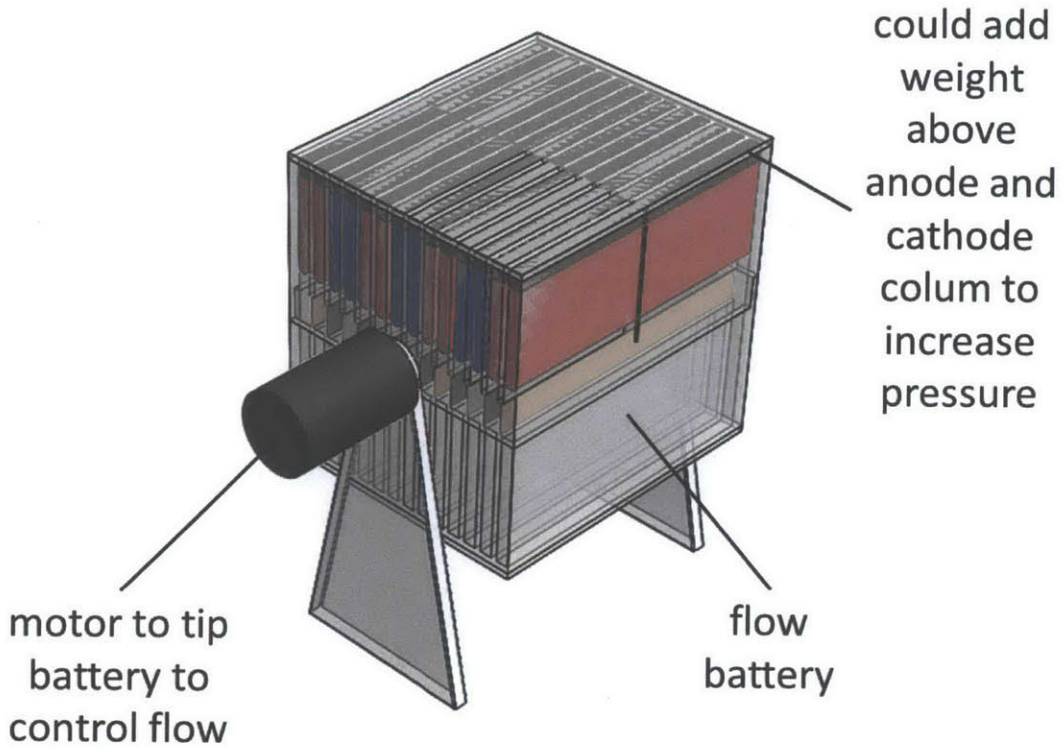

Figure 6.1: Motor on Side of Battery Tilts to Control Flow

High viscosity

1. Pump

Pump the anode and cathode material though the battery just as a conventional flow battery controls flow as shown in Figure 1.3. A plug isolator mechanism could be incorporated into this method of control but would require the pump to run forward and then in reverse.

2. Hydraulic Pistons

Replace the pump with a weight in a hydraulic piston either filled with a gas or with anode and cathode material. The angle of the weight would control the flow of the anode and cathode material. A plug isolator mechanism could be incorporated into this method of control. This method adds weight to the battery, and little pressure is acquired by having a large mass in the hydraulic piston. For example, a 5-inch-tall column of lead only generates 2 psi, and the relationship between column height and pressure scales linearly.

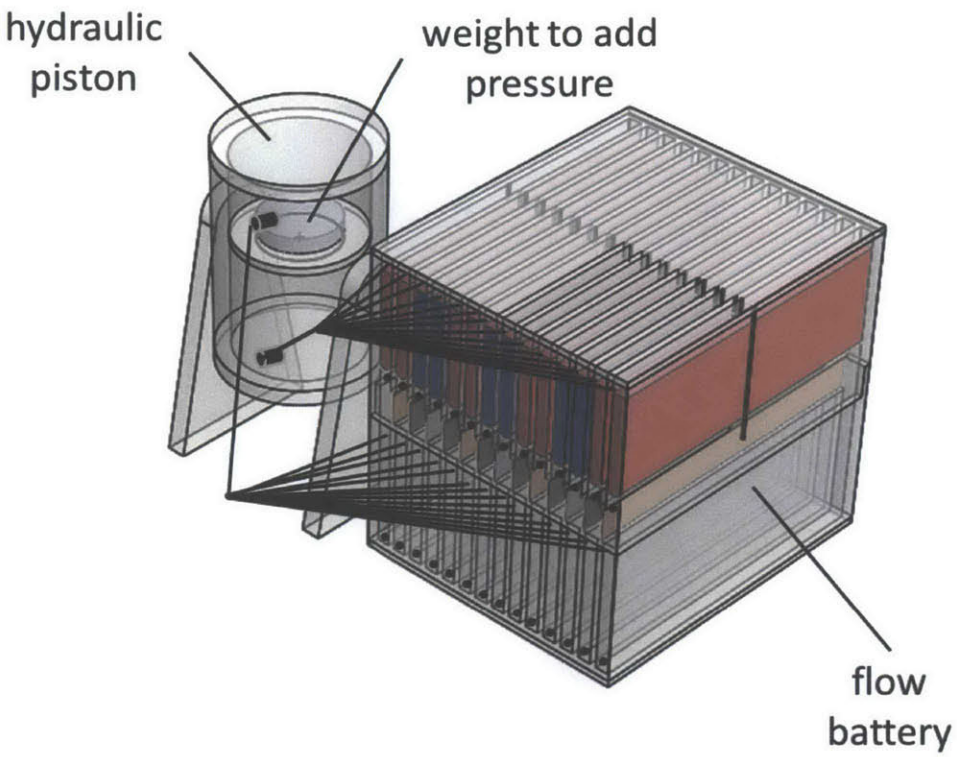

Figure 6.2: Hydraulic Piston with Weight Tilts to Control Flow

4. Compressed Gas

Use compressed gas and control valve to apply pressure to the anode and cathode slurries. A plug isolator mechanism could be incorporated into this method of control. This method of flow control is most likely the lowest weight option as only the weight of the compressed gas chamber is added to the battery. Also the compressed gas can be placed in a small tank with gas held in at high pressures. In terms of efficiency, using compressed gas is essentially like using a pump but the compressed air stores the energy of the pump that was used to compress the air in the tank and then releases it into the battery.

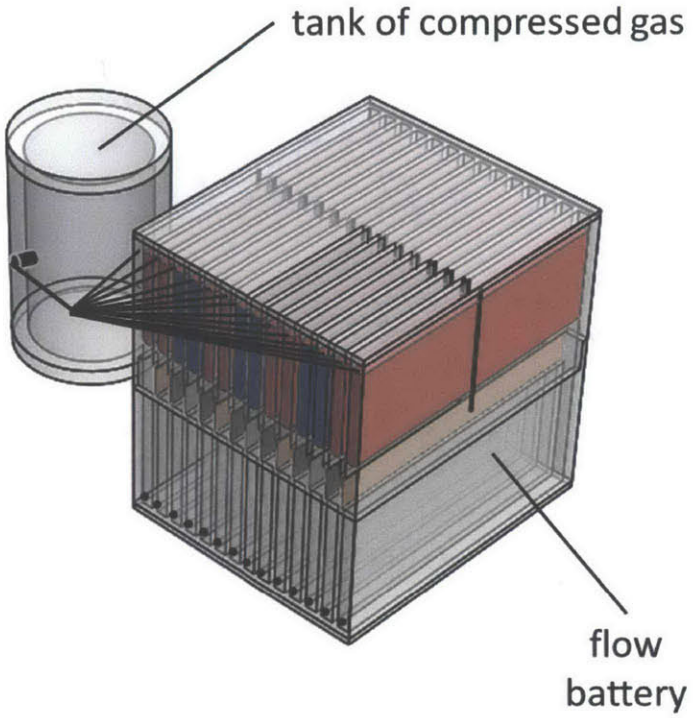

Figure 6.3: Compressed Gas with Control Valve Controls Flow

6.3 Detailed Design

Prototype III was designed and fabricated by Brandon Hopkins. It was 3D printed out of Somos 11122 material. The compressed gas control method with a plug isolator was selected to be demonstrated by the prototype; however, a different type of control method may be appropriate for different situations with different anode and cathode materials. A phantom fluid was used in the battery.

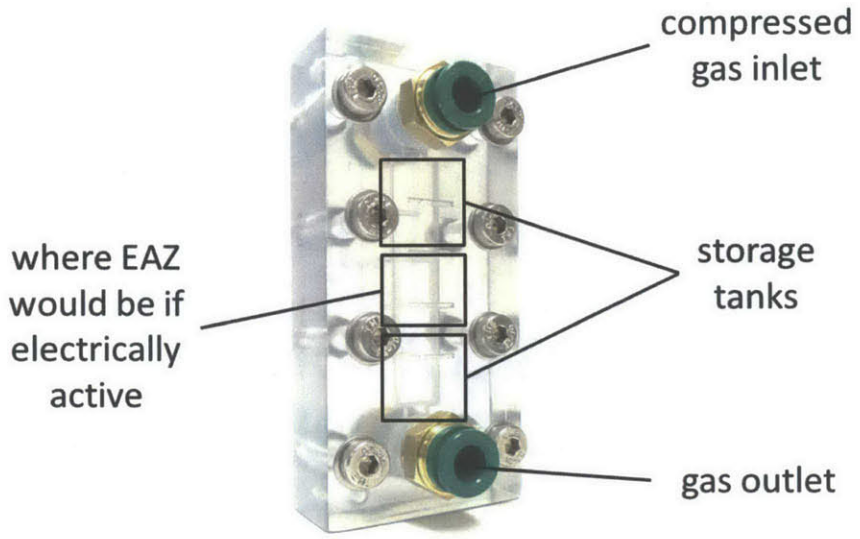

Figure 6.4: Prototype III Compressed Gas Flow Control

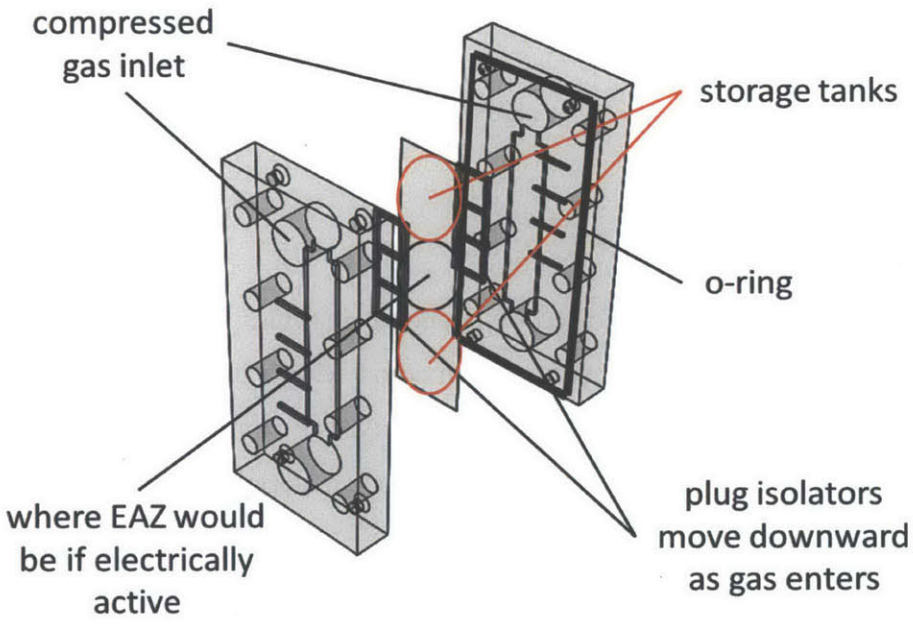

Figure 6.5: Exploded CAD Model of Prototype III

6.4 Testing & Results

Toothpaste was used as the phantom fluid and was placed in the rungs of the plug isolator mechanism. Compressed air was connected to the system to see how well the velocity of the plug isolator could be controlled by the compressed air and to also get an approximation of the amount of pressure required to move the plug isolator and phantom fluid.

Once the compressed air was turned on, the plug isolator did not move until the pressure reached approximately 10 psi. The plug isolator then moved smoothly down in what appeared to be a linear rate. Interestingly, because there were clearance gaps so that the plug isolator could slide freely in the battery, the phantom fluid oozed out of the clearance gaps slightly ahead of the plug isolator mechanism. This problem could be avoided by putting individual seals around every plug isolator section or the clearance of the isolator mechanism could be decreased to minimize the effect

6.5 Chapter Overview

The purpose of Prototype III was to demonstrate how the flow of anode and cathode material in a suspension-based flow battery could be controlled. The method of control is dependent on the amount of pressure required to push the anode and cathode material through the battery. This section presents multiple options for a range of viscosities. Strategies that function for high viscosities also function for low viscosities. The compressed gas strategy could be the most space efficient, and the gravity free fall strategy could be the most energy efficient.

Chapter 7

Conclusion

7.1 Purpose, Importance, and Impact

The purpose of this research is to design low-cost, high-efficiency flow batteries. Researchers are searching for next-generation battery materials but no systems analysis encompassing static and moving electrode architectures has been performed that identifies which architecture is most appropriate for which materials, and how to modify those materials to decrease cost and increase efficiency. The cost model and mechanical designs presented will help researchers (*i*) identify how to modify existing materials, (*ii*) find new desirable materials, and (*iii*) use those materials in novel flow battery structures to create next-generation batteries.

7.2 Accomplishments

According to the author's knowledge, no other cost model or systematic analysis exists that identifies how to determine when a moving electrode architecture is economical given a specific set of battery materials. The presented cost model and analysis is a powerful tool that can focus battery research to quickly determine which materials are worth extensive investigation. This research also presents multiple solutions for a wide range of flow battery materials that will assist in the design of a suspension-based flow battery once an economical set of materials is found.

7.3 Future Work

Given the cost model presented and the multiple options to solve mechanical problems associated with flow batteries, the key obstacle to realizing an economical flow battery may not be mechanical or electrochemical but finding a set of materials that is the economical and feasible. One way of finding such materials would be to rank the top ten studied flow battery chemistries and associated membrane and current collectors based on their economic potential using the cost model and analysis shown in this research and then focus research efforts on those selected materials. According to the author's knowledge, no such ranking has been performed. The electrochemical insights and mechanical solutions discovered in this work could be quickly adapted to meet the needs of newly found materials or new sets or groups of already existing materials that could result in a flow battery with high economic potential.

Appendix

The appendix contains pictures and sketches of battery structures that could be of use in future battery design. The following pictures show how a flow battery could be made into stackable cells.

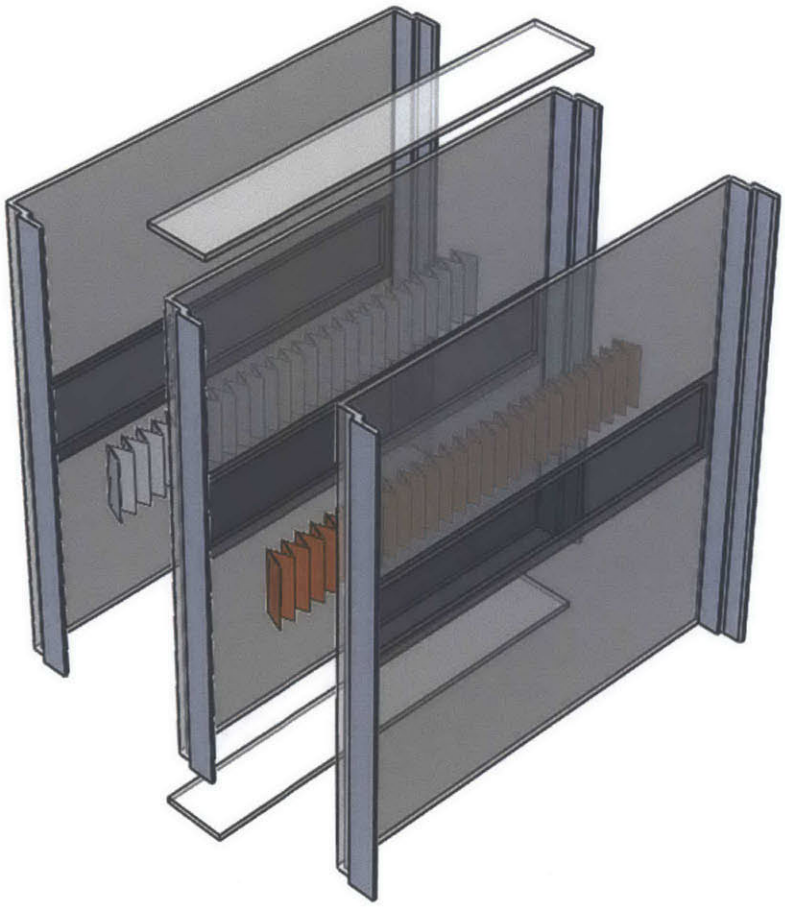

Figure A.1: Stackable Flow Cells

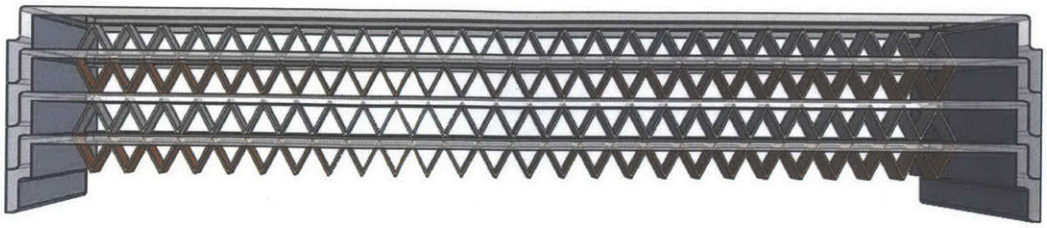

Figure A.2: Detail of Stackable Flow Cells

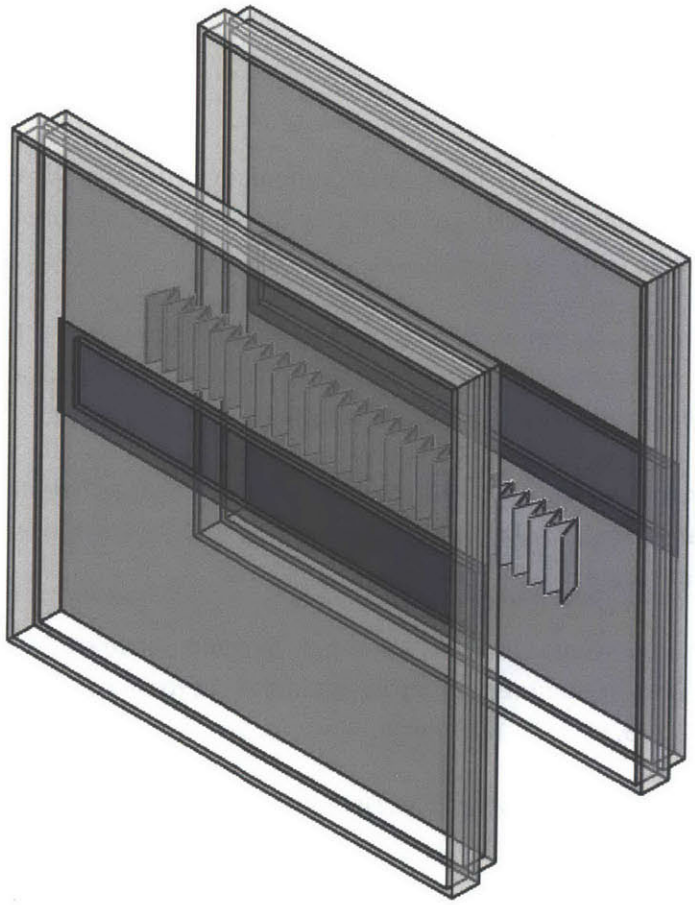

Figure A.3: Stacking Flow Cells with Integrated Bottom and Top Caps

Bibliography

[1] P. Jaramillo, M. W. Griffin and S. H. Mathews, "Comparative Life-Cycle Air Emissions of Coal, Domestic Natural Gas, LNG, and SNG for Electricity Generation," *Environmental Science Technology,* vol. 41, pp. 6290-6296, 2007.

[2] Y. Zhang, J. Mckechnie, D. Cormier, R. Lyng, W. Mabee, A. Ogino and H. L. Maclean, "Life Cycle Emissions and Cost of Producing Electicity from Coal, Natural Gas, Wood, and Pellets in Ontario, Canada," *Environmental Science Technology,* vol. 44, pp. 538-544, 2010.

[3] "Department of Energy Advanced Research Projects Agency Energy, Grid-Scale Rampable Intermittent Dispatchable Storage (GRIDS) Funding Opportunity Announcement," 2010, http://arap-e-foa.energy.gov/..

[4] A. D. Pasquier, I. Plitz, S. Menocal and G. Amatucci, "A comparative study of Li-ion battery, supercapacitor and nonaqueous asymmetric hybrid devices for automotive application," *Journal of Power Sources,* vol. 115, pp. 171-178, 2003.

[5] Y.-M. Chiang, C. W. Carter, B. H. Ho and M. Duduta, "High Energy Density Redox Flow Device," US Pat. 2010/0047671 A1 (2010).

[6] M. Duduta, B. Ho, V. C. Wood, P. Limthongkul, V. E. Brunini, C. W. Carter and Y.-M. Chiang, "Semi-Solid Lithium Rechargeable Flow Battery," *Advanced Energy Materials,* vol. 1, pp. 511-516, 2011.

[7] P. Leung, X. Li, C. Ponce de Leon, B. Leonard, C. T. J. Low and F. C. Walsh, "Progress in redox flow batteries, remaining challenges and their applications in energy storage," *RSC Adances,* vol. 2, pp. 10125-10156, 2012.

[8] W. F. Howard and R. M. Spontnitz, "Theoretical evaluation of high-energy lithium metal phosphate cathode materials in Li-ion batteries," *Journal of Power Sources,* vol. 165, pp. 887-891, 2007.

[9] M. Zhang, M. Moore, T. Zawodzinski and R. M. Counce, "Capital Cost Sensitivity Analysis of an All-Vanadium Redox-Flow Battery," *Journal of The Electrochemical Society,* vol. 159, pp. A1183-A1188, 2012.

[10] M. Skyllas-Kazacos, M. Rychick and R. Robins, "All-Vanadium Redox Battery," US Pat., 4786567 (1988).

[11] M. Skyllas-Kazacos and M. Kazacos, "State of charge monitoring methods for vanadium redox flow battery control," *Journal of Power Sources,* vol. 196 (2011), pp. 8822-8827, 2011.

[12] T. D. J. Hennessy, "Vanadium Redox Battery Energy Storage and Power Generation System Incoporating and Optimizing Diesel Engine Generators," US Pat. 7353083 B2 (2008).

[13] M. Xiangkun, H. Zhang, C. Sun and Y. Z. T. Zou, "An optimal strategy of electrolyte flow rate for vanadium redox flow battery," *Jounral of Power Sources,* vol. 203 (2012), pp. 153-158, 2011.

[14] M. Skyllas-Kazacos and C. Menictas, "The Vanadium Redox Battery for Energy Back-Up Applications," in *Telecommunications Energy Conference*, 1997.

[15] C. R. Horne, K. Kinoshita and D. B. Hickey, "Redox Flow Battery System for Distribution of Energy Storage," US Pat. 7820321 B2 (2010).

[16] Y.-M. Chiang and R. Bazzarella, "Fuel System Using Redox Flow Battery," US Pat. Application Publication 2010/0323264 A1 (2010).

[17] Y.-M. Chiang, W. C. Carter, B. Y. Ho, M. Duduta and P. Limthongkul, "High Energy Density Redox Flow Device," US Pat. Publication 2011/0200848 A1 (2011).

[18] W. C. Young and R. G. Budynas, Roark's Formulas for Stress and Strain, New York: McGraw-Hill, 2002.

[19] C. Hocker, "Design of Semi-Solid Flow Batteries," Massachussetts Institute of Technology, 2012.

[20] A. Zocchi, "Redox Flow Battery and Method of Operating It," US. Pat. 6,692,862 B1, 2004.

[21] J. Boeke, "Multiple Cell Redox Battery," US. Pat 3,540,934, 1970.